THE PLANT CELL

The Plant Cell, 2025, **37**, koae302

https://doi.org/10.1093/plcell/koae302
Advance access publication 13 November 2024
Research Article

The FERONIA-RESPONSIVE TO DESICCATION 26 module regulates vascular immunity to *Ralstonia solanacearum*

Bingqian Wang,[1] Cailin Luo,[1] Xiaoxu Li,[2] Alvaro Jimenez,[3,4] Jun Cai,[1] Jia Chen,[1] Changsheng Li,[1] Chunhui Zhang,[1] Lijun Ou,[5] Wenxuan Pu,[2] Yu Peng,[2] Zhenchen Zhang,[6] Yong Cai,[1,7] Marc Valls,[3,4] Dousheng Wu,[1,7,*] Feng Yu[1,7,*]

[1]State Key Laboratory of Chemo/Biosensing and Chemometrics, and Hunan Key Laboratory of Plant Functional Genomics and Developmental Regulation, College of Biology, Hunan University, Changsha 410082, China
[2]Technology Center, China Tobacco Hunan Industrial Co., Ltd., Changsha 410021, China
[3]Department of Genetics, University of Barcelona, Barcelona, Catalonia 08007, Spain
[4]Centre for Research in Agricultural Genomics (CSIC-IRTA-UAB-UB), Bellaterra, Catalonia 08193, Spain
[5]Engineering Research Center of Education, Ministry for Germplasm Innovation and Breeding New Varieties of Horticultural Crops, Key Laboratory for Vegetable Biology of Hunan Province, College of Horticulture, Hunan Agricultural University, Changsha 410125, China
[6]Guangdong Key Laboratory for Crops Genetic Improvement, Crops Research Institute, Guangdong Academy of Agricultural Sciences (GAAS), Guangzhou 510640, China
[7]Yuelushan Laboratory, Changsha 410128, China
*Author for correspondence: feng_yu@hnu.edu.cn (F.Y.), dousheng.wu@hnu.edu.cn (D.W.)
The author responsible for distribution of materials integral to the findings presented in this article in accordance with the policy described in the Instructions for Authors (https://academic.oup.com/plcell/pages/General-Instructions) is Feng Yu (feng_yu@hnu.edu.cn).

Abstract

Some pathogens colonize plant leaves, but others invade the roots, including the vasculature, causing severe disease symptoms. Plant innate immunity has been extensively studied in leaf pathosystems; however, the precise regulation of immunity against vascular pathogens remains largely unexplored. We previously demonstrated that loss of function of the receptor kinase FERONIA (FER) increases plant resistance to the typical vascular bacterial pathogen *Ralstonia solanacearum*. Here, we show that upon infection with *R. solanacearum*, root xylem cell walls in *Arabidopsis thaliana* become highly lignified. FER is specifically upregulated in the root xylem in response to *R. solanacearum* infection, and inhibits lignin biosynthesis and resistance to this pathogen. We determined that FER interacts with and phosphorylates the transcription factor RESPONSIVE TO DESICCATION 26 (RD26), leading to its degradation. Overexpression and knockout of *RD26* demonstrated that it positively regulates plant resistance to *R. solanacearum* by directly activating the expression of lignin-related genes. Tissue-specific expression of *RD26* in the root xylem confirmed its role in vascular immunity. We confirmed that the FER–RD26 module regulates lignin biosynthesis and resistance against *R. solanacearum* in tomato (*Solanum lycopersicum*). Taken together, our findings unveil that the FER–RD26 cascade governs plant immunity against *R. solanacearum* in vascular tissues by regulating lignin deposition. This cascade may represent a key defense mechanism against vascular pathogens in plants.

Introduction

Plants have developed a two-layered immune system to detect and combat pathogens. The first layer, called PAMP-triggered immunity (PTI), is activated when pattern recognition receptors (PRRs) located at the cell surface recognize pathogen-associated molecular patterns (PAMPs). The second layer, known as effector-triggered immunity (ETI), is activated when intracellular nucleotide-binding domain leucine-rich repeat-containing receptors (NLRs) detect pathogen effectors (Chisholm et al. 2006; Jones and Dangl 2006). Substantial progress has been made over the past two decades in understanding the recognition mechanisms and downstream signaling events of PTI and ETI (Yuan et al. 2021; Chang et al. 2022), particularly for pathogens infecting their hosts through leaves. Although PTI and ETI also play a role in plant interactions with vascular pathogens, there has been limited research specifically analyzing these interactions in the xylem of infected plants (Kashyap et al. 2021). Considering the notable differences between mesophyll cells and xylem cells, it is plausible that plants employ specific mechanisms to regulate resistance or immunity in the xylem tissue that would have been missed when characterizing leaf pathogens.

Xylem-invading pathogens pose a major threat to plants as they proliferate within the xylem, producing toxins and exopolysaccharides that block water transport, which results in severe wilting and eventual plant death (Kashyap et al. 2021; De La Fuente et al. 2022). To defend against these pathogens, plants have developed complex physicochemical barriers within the xylem tissue. One defense mechanism is the deposition of lignin, creating a physical barrier that limits pathogen colonization. Lignin is involved not only in basal immune responses (Chezem et al. 2017) but also in ETI (Cui et al. 2015; Lee et al. 2019; Kim et al. 2020; Jeon et al. 2023). Lignin-related genes are transcriptionally upregulated in resistant plants after inoculation with vascular pathogens (Ishihara et al. 2012; Galindo-González and Deyholos 2016; Sabella et al. 2018). Increased lignin content correlates with greater plant resistance to vascular pathogens (Ferreira et al. 2017; Novo et al. 2017). Despite the importance of lignin in resistance to vascular pathogens, the upstream regulators and signaling pathways controlling lignin deposition during pathogen invasion remain largely unknown. A recent study discovered a conserved signaling cascade consisting of MITOGEN-ACTIVATED PROTEIN KINASE PHOSPHATASE 1 (MPK1),

Received April 23, 2024. Accepted November 6, 2024

a MITOGEN-ACTIVATED PROTEIN KINASE (MAPK), and a MYB-type transcription factor, that activates lignin biosynthesis in vascular tissues, providing vascular resistance in both rice (*Oryza sativa*) and Arabidopsis (*Arabidopsis thaliana*) (Lin et al. 2022).

The malectin-like receptor kinase FERONIA (FER) is a member of the *Catharanthus roseus* receptor-like kinase 1-like family (CrRLK1L) and plays multiple roles in regulating plant growth, as well as in abiotic and biotic stress responses (Chen et al. 2016; Zhang et al. 2020b; Zhu et al. 2021). Depending on the plant tissues and pathogens involved, FER can either positively or negatively regulate plant immunity (Stegmann et al. 2017; Guo et al. 2018; Zhang et al. 2020a). It has been proposed that FER acts as a scaffold, facilitating the assembly of immune receptor complexes, thereby positively regulating plant immunity (Stegmann et al. 2017). FER is also involved in sensing cell wall softening and maintaining cell wall integrity (Feng et al. 2018). The cell wall is a complex structure that pathogens must break through for a successful infection, making it a crucial component of plant defense against pathogens. FER, along with cell wall-associated kinases, can coordinate plant defense by modulating lignin modifications in plant cell walls (Liu et al. 2023a).

Bacterial wilt, caused by the bacterium *Ralstonia solanacearum*, is a destructive vascular plant disease. This pathogen invades the cortical tissue of host roots, blocks the xylem, and ultimately leads to stunted growth and deadly wilt in the host plant (Lowe-Power et al. 2018). *Ralstonia solanacearum* can infect over 250 plant species, including various Solanaceae species such as tomato (*Solanum lycopersicum*), potato (*Solanum tuberosum*), pepper (*Capsicum annuum*), and eggplant (*Solanum melongena*). *Ralstonia solanacearum* is considered the world's second most important phytopathogenic bacterium (after *Pseudomonas syringae*), owing to its substantial scientific and economic impact (Mansfield et al. 2012). To successfully infect host plants, *R. solanacearum* uses various pathogenicity factors, including Type II and Type III secretion systems. These systems secrete cell wall-degrading enzymes such as pectic lyases and cellulases into the extracellular space, as well as Type III effectors into host cells, to facilitate infection (Poueymiro and Genin 2009; Genin and Denny 2012). The colonization of the vascular tissue by *R. solanacearum* makes the molecular study of bacterial wilt resistance rather challenging owing to the limited access to these cells. We previously showed that mutation of *FER* or inhibition of FER-kinase activity enhances plant resistance to *R. solanacearum* (Liu et al. 2023b), but the molecular mechanisms underlying FER-mediated resistance to bacterial wilt remain to be determined.

Here, we demonstrate that cell wall lignification increases in the root xylem in response to *R. solanacearum* infection. We reveal that FER negatively regulates lignin biosynthesis in the xylem. FER physically interacts with and degrades RESPONSIVE TO DESICCATION 26 (RD26, also reported as NAC072), a NAC transcription factor belonging to the ATAF subfamily (Fujita et al. 2004), which otherwise positively regulates plant resistance to *R. solanacearum* by activating the expression of genes involved in lignin deposition. The FER–RD26 module sheds light on the mechanisms underlying plant resistance to the vascular pathogen *R. solanacearum*, providing valuable insights for future vascular immunity studies and breeding of disease-resistant crops.

Results

Plants enhance cell wall lignification in their xylem in response to *R. solanacearum* infection

To confirm the colonization of the root xylem of Arabidopsis seedlings by *R. solanacearum*, we inoculated Arabidopsis seedlings with a green fluorescent protein (GFP)-labeled *R. solanacearum* strain (GMI1000-*GFP*, Phylotype I) (Zhou et al. 2020) and visualized the roots using fluorescence microscopy (Supplementary Fig. S1A). We observed clear GFP signal in the root xylem of infected seedlings, indicating successful colonization of the pathogen (Fig. 1A, Supplementary Fig. S1B). We then investigated the plant defense response against *R. solanacearum* in the xylem tissue, focusing on cell wall lignification, which is a crucial component of vascular immunity (Kashyap et al. 2021; Lin et al. 2022). Accordingly, we stained lignin in the roots with phloroglucinol-hydrochloric acid (HCl) staining and quantified the lignin content by the acetyl bromide-based method, which revealed a significantly higher level of lignin accumulation at 12 h post inoculation (hpi) with *R. solanacearum* in the xylem of infected Arabidopsis roots than in those of mock-inoculated seedlings (Fig. 1, B and C). In addition, lignin accumulation was more pronounced in the vicinity of infected areas (Fig. 1D). We also examined the expression of *PHENYLALANINE AMMONIA-LYASE 1* (*PAL1*), a gene involved in lignin biosynthesis, using the *proPAL1:PAL1-VENUS* reporter line (Xue et al. 2020). *PAL1* expression was substantially increased in the xylem after *R. solanacearum* inoculation (Fig. 1E). Collectively, these findings demonstrate that seedlings increase their cell wall lignification as a defense mechanism against *R. solanacearum* in the xylem.

FER is involved in the regulation of lignin biosynthesis in response to *R. solanacearum* infection in the xylem

Our recent study unveiled a role for the receptor kinase FER in plant resistance to *R. solanacearum* (Liu et al. 2023b). Additionally, FER was shown to regulate defense responses in response to altered cell wall composition (Liu et al. 2023a). Therefore, we hypothesized that FER might be implicated in cell wall lignification in response to *R. solanacearum* infection. We determined that the *fer-4* mutant (Duan et al. 2010) is more resistant to *R. solanacearum* infection than the wild-type Col-0 (Supplementary Fig. S2, A to E). *FER* transcript levels were similar in the roots of mock-treated and GMI1000-inoculated seedlings (Supplementary Fig. S2F). suggesting that *R. solanacearum* inoculation has no impact on *FER* transcription. We then took advantage of a transgenic line expressing *FER-GFP* under the control of its native promoter (*proFER:FER-GFP*) (Duan et al. 2010). FER protein abundance was higher in the root xylem of *proFER:FER-GFP* seedlings upon *R. solanacearum* inoculation (Fig. 2A), indicating a role for FER in root xylem in response to *R. solanacearum* infection. To assess cell wall lignification, we stained and quantified the lignin content in the roots of Col-0 and *fer-4* seedlings. In mock-inoculated seedlings, *fer-4* exhibited higher lignin levels in the xylem than did in Col-0 (Fig. 2, B and C). Furthermore, the lignin content increased to a greater extent in *fer-4* in response to *R. solanacearum* infection than in Col-0 (Fig. 2, B and C). These results indicate that FER acts as a negative regulator of lignin biosynthesis in the xylem during *R. solanacearum* invasion.

We further examined the colonization of *R. solanacearum* in the xylem of Col-0 and *fer-4* roots, which revealed impaired bacterial colonization in the *fer-4* xylem compared to Col-0 (Fig. 2D). To further confirm the role of FER in bacterial wilt resistance and lignin regulation, we evaluated the disease phenotype of the other Arabidopsis accession C24 and *sirène* (*srn*) (Rotman et al. 2003; Duan et al. 2010), an independent mutant of *FER* in the C24 background. To this end, we inoculated C24 and *srn* seedlings grown on plates for an in vitro inoculation assay; similar to *fer-4*, *srn* exhibited increased resistance to *R. solanacearum* infection, as evidenced by the more modest inhibition of root elongation observed in the mutant following

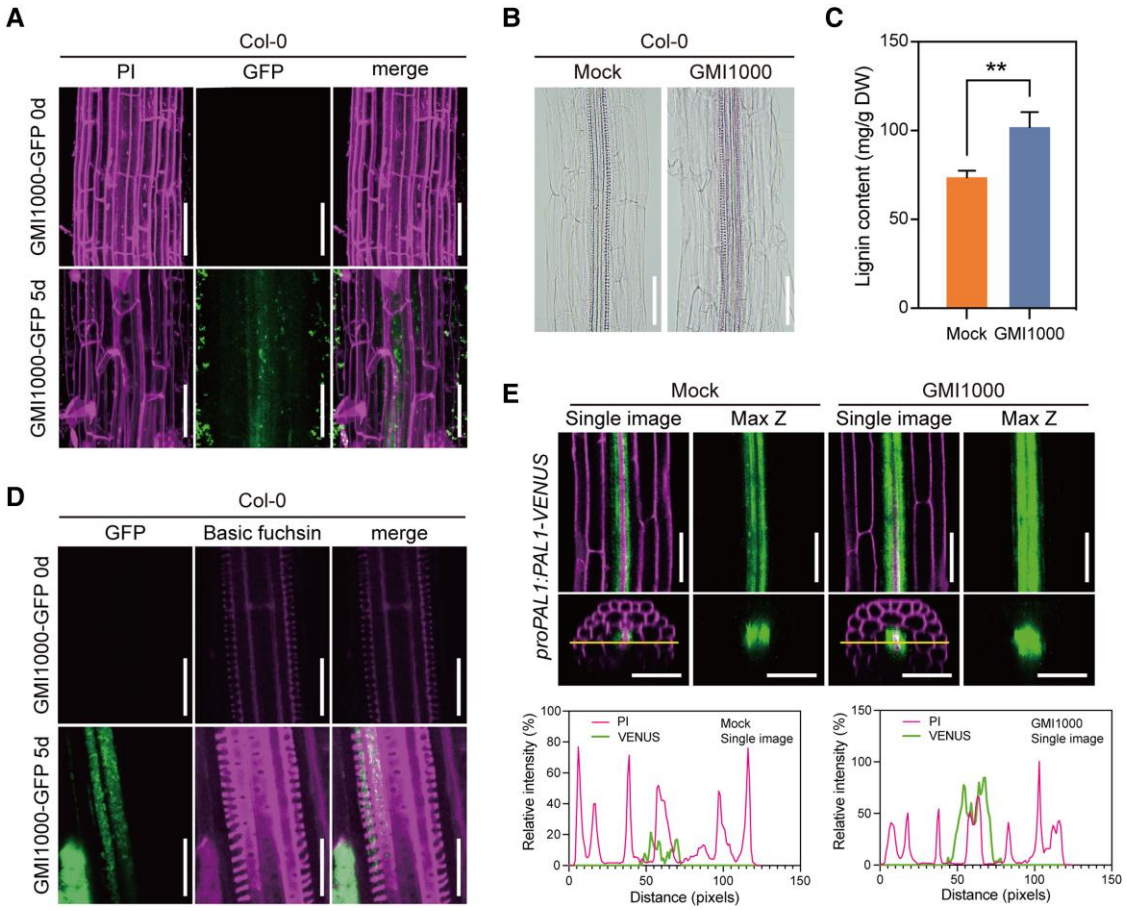

Figure 1. Cell wall lignification in the xylem of Arabidopsis roots in response to *R. solanacearum* infection. **A)** Colonization of vascular bundles by *R. solanacearum* in Col-0 roots. Seven-day-old seedlings were inoculated with 10 μL of a bacterial suspension of a GFP-labeled *R. solanacearum* strain (GMI1000-*GFP*) at a titer of 1×10^7 CFUs/mL. Photographs were taken at 0 and 5 dpi. Green indicates GFP signal. Magenta indicates PI staining of the cell walls. Scale bars, 50 μm. **B** and **C)** Lignin visualization **(B)** and quantification **(C)** in the xylem of Arabidopsis roots at 12 h post inoculation (hpi) with *R. solanacearum*. The roots were stained with phloroglucinol-hydrochloric acid (HCl) at 12 hpi with *R. solanacearum* and the lignin content was quantified by the acetyl bromide-based method. Scale bars, 50 μm. DW, dry weight (oven drying). Values are means ± SD ($n = 3$). $^{**}P < 0.01$ (Student's *t*-test). **D)** Simultaneous visualization of *R. solanacearum* colonization (based on GFP fluorescence) and lignification in the vascular cylinder of Arabidopsis roots. Col-0 seedlings were inoculated with the *R. solanacearum* GMI1000-*GFP* strain; lignin was stained with basic fuchsin at 5 dpi. Scale bars, 20 μm. Green represents GFP signals. Magenta indicates staining of lignin with basic fuchsin. **E)** Spatial *PAL1* expression pattern in response to *R. solanacearum* inoculation. The *proPAL1:PAL1-VENUS* reporter line was inoculated with *R. solanacearum*; the GFP signal was observed at 12 hpi. In each treatment, single confocal sections (single image, left) and maximal projections of Z-stacks (Max Z, right) are shown; median longitudinal and transverse section views are shown on the top and bottom, respectively. Green indicates VENUS signal. Magenta indicates PI staining of cell walls. Scale bars, 50 μm. GFP and PI fluorescence intensities along the yellow lines in the transverse sections are shown below the confocal images. All experiments were performed 3 times with similar results.

infection (Supplementary Fig. S3, A and B). This result validates the negative role of FER in plant resistance to *R. solanacearum*. Phloroglucinol-HCl staining and quantification of lignin content showed that lignin accumulates to higher levels in *srn* in response to *R. solanacearum* infection than it does in C24 (Supplementary Fig. S3, C and D). The greater deposition of lignin in the root xylem of *srn* seedlings was associated with diminished colonization by *R. solanacearum* (Supplementary Fig. S3E). In summary, these findings suggest that increased lignin deposition confers resistance to *R. solanacearum*, while FER suppresses lignin accumulation in the xylem and negatively regulates plant resistance to *R. solanacearum*.

FER interacts with the NAC transcription factor RD26

To unravel the molecular mechanism by which FER regulates lignin biosynthesis, we searched for interacting proteins of FER. Accordingly, we performed a yeast two-hybrid (Y2H) screen using a truncated version (amino acids [aa] 492 to 895) of FER (FER-KD) corresponding only to the kinase domain as bait against an Arabidopsis cDNA library (Du et al. 2016). We identified one clone encoding a fragment (aa 110 to 297) of NAC072, also reported as RD26, as a candidate interactor. RD26 belongs to the NAC transcription factor family. Some members of the NAC family have been shown to regulate lignin deposition in Arabidopsis (Liu et al. 2021).

We confirmed the interaction between FER-KD and full-length RD26 by targeted Y2H (Fig. 3A). We also purified recombinant His-FER-KD and glutathione S-transferase (GST)-tagged RD26 and performed GST pull-down assays to assess their direct binding in vitro. Indeed, GST-RD26 was able to bind to His-FER-KD in vitro (Fig. 3B). To validate the FER–RD26 interaction in planta, we cloned the full-length *RD26* coding sequence in-frame and upstream of the sequence encoding the N-terminal half of firefly luciferase (NLUC); we cloned the sequence encoding FER-KD or full-length FER in-frame and downstream of the sequence encoding the C-terminal half of LUC (CLUC) to perform a luciferase complementation

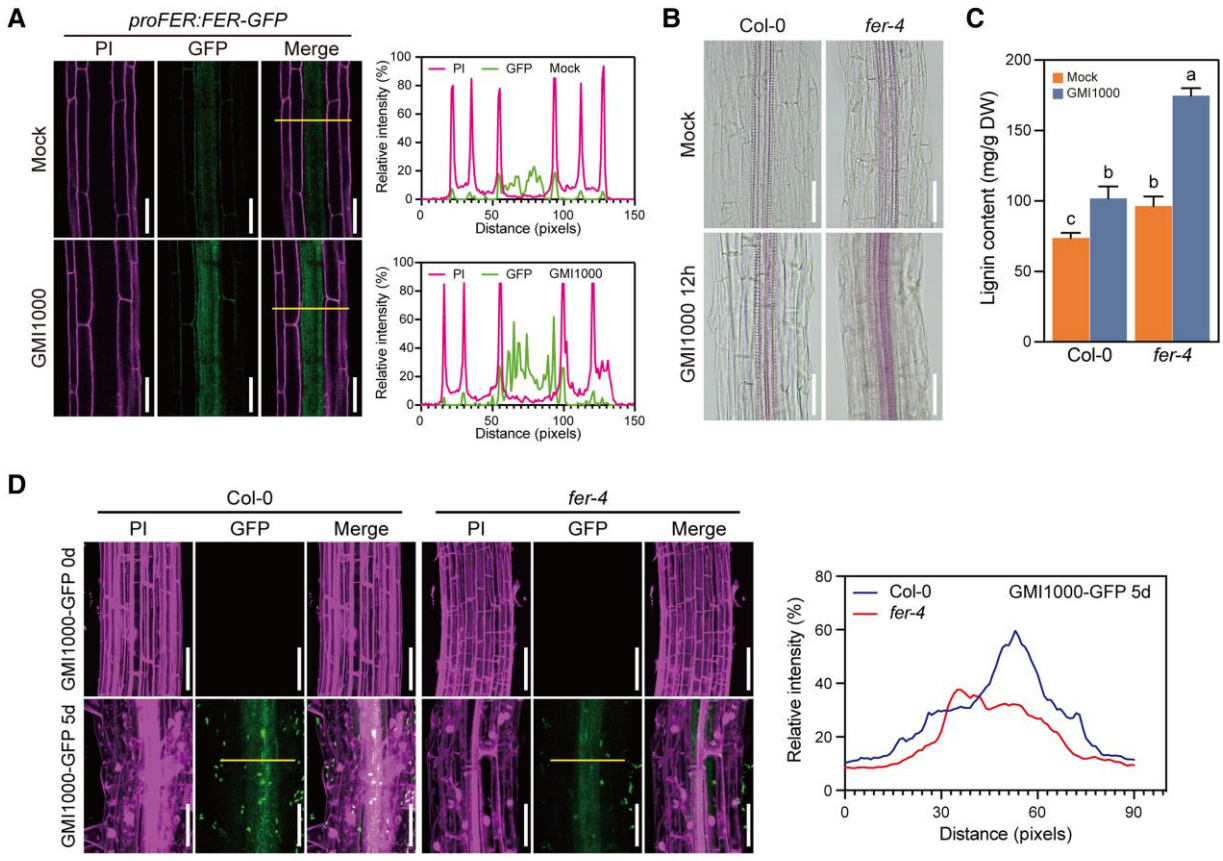

Figure 2. FER is involved in lignification of the Arabidopsis root xylem upon *R. solanacearum* infection. **A)** Spatial expression pattern of *FER* in response to *R. solanacearum* infection. The *proFER:FER-GFP* reporter line was inoculated with GMI1000 or with sterile water (Mock). Confocal microscopy images were taken at 12 hpi. Green represents GFP signals. Magenta indicates PI staining of the cell walls. Scale bars, 50 μm. Quantification of the GFP and PI fluorescence signal in the *proFER:FER-GFP* reporter line after inoculation with *R. solanacearum* along the orange lines is shown to the right. **B** and **C)** Lignin visualization **(B)** and quantification **(C)** in the xylem of Arabidopsis roots after inoculation with *R. solanacearum*. Col-0 and *fer-4* roots were stained with phloroglucinol-HCl at 12 hpi with *R. solanacearum*. Scale bars, 50 μm. DW, dry weight (oven drying). Values are means ± SD ($n = 3$). Different lowercase letters indicate significant differences by one-way ANOVA ($P < 0.05$). **D)** Colonization of vascular bundles by *R. solanacearum* in Col-0 and *fer-4* roots. Seven-day-old seedlings were inoculated with GMI1000-*GFP* at a titer of 10 μL of 1×10^7 CFUs/mL. Photographs were taken at 5 dpi. Green indicates GFP signal. Magenta indicates PI staining of the cell walls. Scale bars, 50 μm. GFP fluorescence intensities along the yellow lines in the median longitudinal sections are shown to the right. All experiments were performed 3 times with similar results.

imaging (LCI) assay. We co-infiltrated *Nicotiana benthamiana* leaves with mixtures of Agrobacterium (*Agrobacterium tumefaciens*) cultures harboring *CLUC-FER-KD* or full-length *CLUC-FER* with *RD26-NLUC*. In both cases, we detected high luciferase activity (Fig. 3C), indicating a strong interaction between FER (truncated to the kinase domain and full-length) and RD26. We confirmed the FER–RD26 interaction in vivo through co-immunoprecipitation (Co-IP) assays using total protein extracts from *35S:RD26-GFP* seedlings and an anti-FER antibody (Fig. 3D).

FER belongs to the CrRLK1L family and shares high similarity with other members. To explore the possible interaction of RD26 with several FER homologs, we conducted Y2H assays using RD26 as bait and the kinase domain of FER or the candidate CrRLK1L as prey. We only detected a specific interaction between FER-KD and RD26 (Supplementary Fig. S4).

Ralstonia solanacearum colonizes the root xylem for bacterial proliferation (Fig. 1A) and *FER* expression was strongly induced in the xylem upon *R. solanacearum* infection (Fig. 2A). We hypothesized that the FER–RD26 interaction might take place in the xylem. To test this hypothesis, we generated complementation lines harboring a transgene consisting of *VENUS* cloned in-frame and downstream of full-length *RD26* and driven by the xylem-specific promoter from *MAGNESIUM TRANSPORTER 6* (*MGT6*) (Meng et al. 2022) in the *rd26* background (*rd26 proMGT6:RD26-VENUS*). Confocal microscopy observations confirmed the specific expression of *RD26* in xylem parenchyma cells (Supplementary Fig. S5). We then carried out Co-IP assays with the *rd26 proMGT6:RD26-VENUS* line, using an anti-FER antibody. RD26-VENUS successfully co-precipitated with FER (Fig. 3E), indicating that FER and RD26 interact in the root xylem.

FER phosphorylates RD26 to promote its degradation

Being a receptor-like kinase, FER regulates various cellular programs by phosphorylating its substrates. Given the direct interaction between FER and RD26, we asked whether RD26 might serve as a substrate for FER. We therefore performed in vitro kinase assays using purified recombinant GST-RD26, His-FER-KD, and His-FER^{K565R}-KD, a kinase-dead version of FER (Xu et al. 2024). We used an antibody that specifically recognizes phosphorylated serine and threonine residues (anti-pSer/anti-pThr) to probe each protein mixture: we detected the phosphorylation of GST-RD26 in the presence of His-FER-KD but not with His-FER^{K565R}-KD, suggesting that FER can phosphorylate RD26 in vitro (Fig. 4A). Furthermore, immunoprecipitation of RD26 produced from *35S:RD26-MYC* transgenic seedlings using MYC-trap beads followed by immunoblotting with the

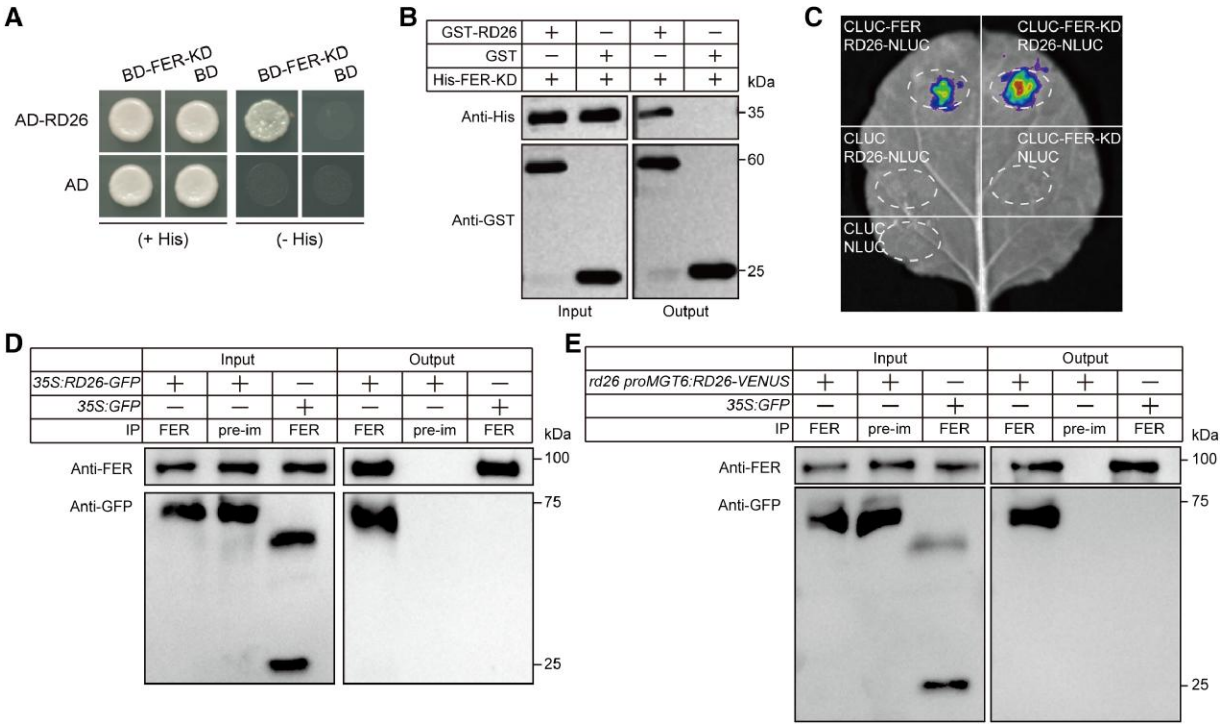

Figure 3. FER interacts with RD26 in vitro and in vivo. **A)** Yeast two-hybrid assay confirming the interaction between FER and RD26. The full-length *RD26* coding sequence was cloned into the pGADT7 (AD) vector and the sequence encoding FER-kinase domain (FER-KD) was cloned into the pGBKT7 (BD) vector. The *RD26* and *FER-KD* constructs were co-transformed into yeast and transformants were selected on synthetic defined (SD) medium lacking leucine and tryptophan (+His). Protein–protein interaction was tested on SD medium lacking leucine, tryptophan, and histidine and containing 20 mM 3-AT (-His). The empty vectors AD and BD were used as negative controls. **B)** GST pull-down assay. Recombinant GST-RD26 and His-FER-KD were produced in *E. coli*, purified, and co-incubated, followed by pull-down with glutathione beads. RD26 and FER-KD were detected by immunoblot analysis with anti-GST and anti-His antibodies, respectively. **C)** Luciferase complementation imaging (LCI) assay. *Agrobacterium tumefaciens* cell suspensions each harboring one of the indicated constructs were mixed and infiltrated into *N. benthamiana* leaves; luciferase activity was examined with a charge-coupled device (CCD) camera at 2 days post infiltration. **D)** Co-immunoprecipitation (Co-IP) assay. FER was immunoprecipitated with anti-FER antibodies. Co-immunoprecipitated RD26 was detected using anti-GFP antibodies. *35S:GFP* and preimmune mouse serum (pre-im) against *35S:RD26-GFP* were used as negative controls in the Co-IP assay. **E)** Co-IP assay using *rd26 proMGT6:RD26-VENUS* expressing *RD26-VENUS* from the xylem-specific *MGT6* promoter. The immunoprecipitated FER and co-immunoprecipitated RD26 were detected using anti-FER and anti-GFP antibodies, respectively. All experiments were performed 3 times with similar results.

anti-pSer/anti-pThr antibody revealed higher phosphorylation levels for RD26 in *35S:RD26-MYC* roots than in *fer-4 35S:RD26-MYC* roots (Fig. 4B), indicating that FER is one of the kinases that phosphorylates RD26 in vivo. We identified the FER-mediated phosphorylation sites of RD26 through liquid chromatography–tandem mass spectrometry (LC-MS/MS) analysis of the in vitro reaction products of GST-RD26 incubated with His-FER-KD. FER-KD phosphorylated RD26 at the residues Ser-61, Ser-92, Ser-182, Ser-263, Ser-273, and Thr-292 in vitro (Supplementary Fig. S6). We mutated these six phosphorylation sites in RD26 to alanine residues ($RD26^{mutA}$). An in vitro kinase assay revealed that mutation of these phosphorylation sites nearly completely abolishes FER-KD-mediated RD26 phosphorylation (Fig. 4A), demonstrating that the phosphorylation of RD26 by FER indeed takes place at these serine and threonine residues.

To assess the effect of FER phosphorylation on RD26 protein stability in vivo, we cloned the full-length *RD26* sequence in-frame and upstream of *LUC*, with the expression of *RD26-LUC* driven by the 35S promoter; we transfected the resulting reporter into Col-0 and *fer-4* protoplasts. The luciferase activity derived from the RD26-LUC fusion was clearly higher in *fer-4* than in Col-0 (Fig. 4C), indicating that FER promotes RD26 degradation. Co-expression of *RD26-MYC* with *FER-KD-GFP* in *N. benthamiana* leaves also resulted in decreased RD26 abundance compared to that in the presence of FER^{K565R}-KD-GFP (Supplementary Fig. S7A).

We further performed a cell-free degradation assay by incubating recombinant purified GST-RD26 with plant protein extracts. Under these conditions, GST-RD26 was more stable in *fer-4* extracts than in Col-0 extracts (Fig. 4D). In another set of cell-free degradation assays, we incubated total protein extracts from Col-0 and recombinant purified GST-RD26 or its nonphosphorylatable variant GST-$RD26^{mutA}$ or the phosphorylation-mimic variant GST-$RD26^{mutD}$ with the six phosphorylation sites changed to aspartic acid. The degradation of GST-$RD26^{mutA}$ was slower than that of GST-RD26, while the degradation of GST-$RD26^{mutD}$ was faster (Supplementary Fig. S7B), confirming the phosphorylation-dependent degradation of RD26. To validate this observation, we assessed the protein stability of RD26-GFP and $RD26^{mutA}$-GFP in Col-0 and *fer-4* by Agrobacterium-mediated infiltration of the encoding constructs in Arabidopsis leaves. RD26-GFP was more stable in the leaves of *fer-4* than Col-0, whereas $RD26^{mutA}$-GFP exhibited a similar stability in Col-0 and *fer-4* (Supplementary Fig. S7C), suggestive of FER-mediated RD26 degradation. Moreover, protein quantification after treatment with the translation inhibitor cycloheximide (CHX) revealed a longer half-life for RD26 in the *fer-4* mutant (Supplementary Fig. S7D).

Gene expression databases indicate that *RD26* is predominantly expressed in the vasculature of Arabidopsis roots (Supplementary Fig. S7E) (Fucile et al. 2011). We generated a transgenic line expressing *RD26-VENUS* under its native promoter

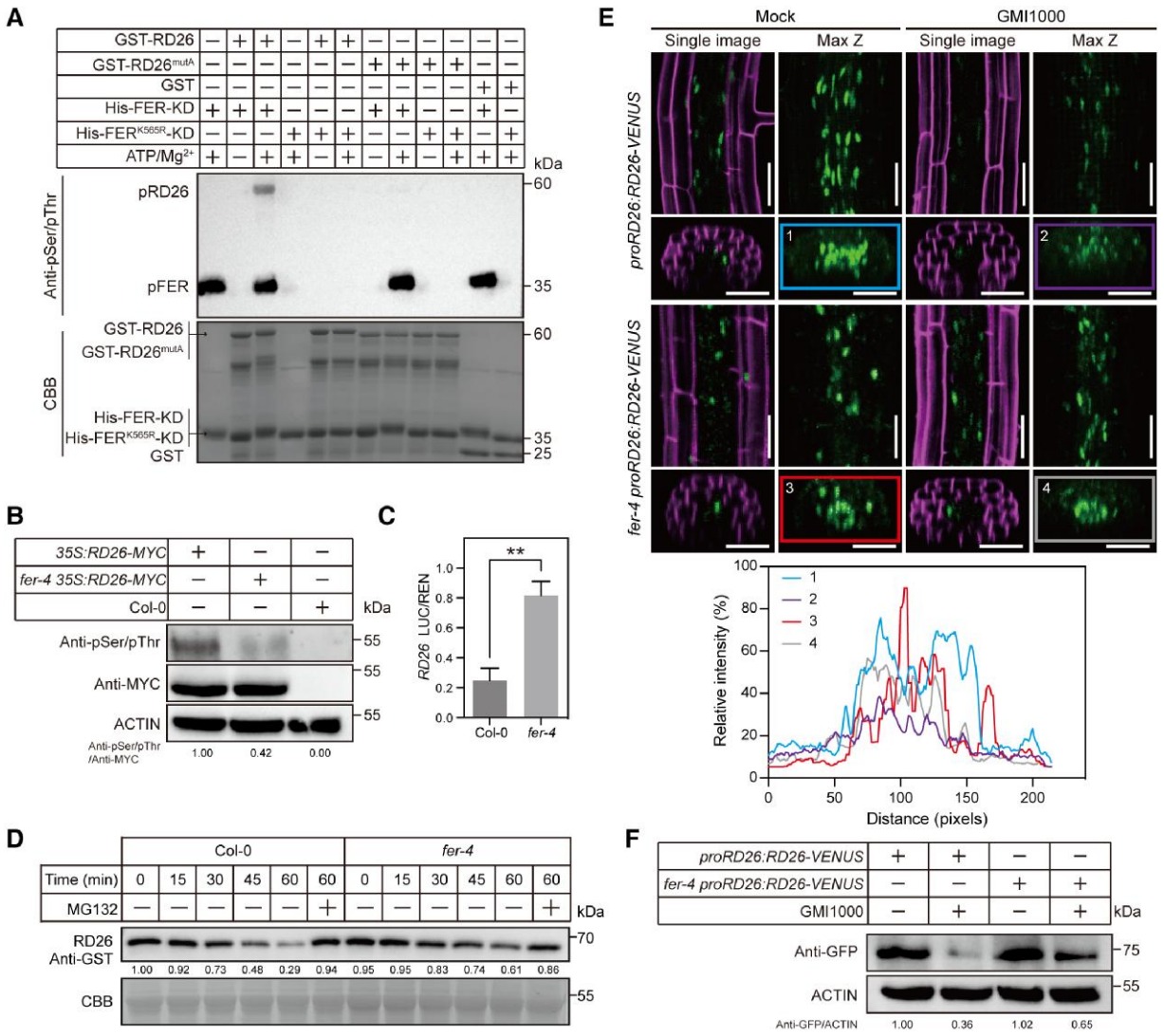

Figure 4. FER phosphorylates and regulates the stability of RD26. **A** and **B)** FER phosphorylates RD26. **A)** In vitro phosphorylation assay showing that recombinant purified His-FER-KD can phosphorylate GST-RD26. KD, kinase domain. Phosphorylation levels were detected with anti-pSer/pThr antibodies. FER and RD26 were detected by CBB staining of the SDS-PAGE gels. **B)** FER phosphorylates RD26 in vivo. Seven-day-old Arabidopsis seedlings of *35S:RD26-MYC*, *fer-4 35S:RD26-MYC*, and Col-0 were used for in vivo phosphorylation assay. RD26 phosphorylation levels were detected with anti-pSer/pThr. RD26 was detected with anti-MYC antibodies. **C)** RD26 is more stable in *fer-4* than in Col-0, based on a dual-luciferase reporter assay. The full-length *RD26* coding sequence was cloned in-frame and upstream of the firefly luciferase (*LUC*) reporter gene, and driven by the cauliflower mosaic virus (CaMV) *35S* promoter. Renilla luciferase (*REN*) driven by the *35S* promoter was used as infiltration control. The resulting constructs were transformed into Col-0 and *fer-4* root protoplasts. Values are means ± SD ($n = 3$). The significance of differences was evaluated using Student's *t*-test (**$P < 0.01$). **D)** RD26 protein is more stable in *fer-4*, as shown by a cell-free degradation assay. Recombinant purified RD26 was mixed with total protein extracted from Col-0 or *fer-4* seedlings. RD26 was detected with anti-GST antibodies. MG132 is a commonly used proteasome inhibitor. CBB, Coomassie Brilliant Blue staining. Quantification was carried out using FIJI. **E)** Spatial expression pattern of *RD26* in the roots of *proRD26:RD26-VENUS* and *fer-4 proRD26:RD26-VENUS* seedlings in response to *R. solanacearum* inoculation. Arabidopsis seedlings were inoculated with a GMI1000 bacterial suspension at a titer of 10 μL of 1×10^7 CFUs/mL. Single confocal sections (single image, left) and maximal projections of Z-stacks (Max Z, right) are shown; median longitudinal and transverse section views are shown on the top and bottom, respectively. Green indicates VENUS signals; Magenta indicates PI staining of the cell walls. Scale bars, 50 μm. Quantification of the VENUS fluorescence signal in transverse section after inoculation with *R. solanacearum* is shown below. **F)** Protein abundance of RD26 in the roots of *proRD26:RD26-VENUS* and *fer-4 proRD26:RD26-VENUS* seedlings in response to *R. solanacearum* infection. RD26 in roots was detected using anti-GFP antibodies. Quantification was carried out using FIJI. All experiments were performed 3 times with similar results.

(*proRD26:RD26-VENUS*) in the Col-0 background and observed strong fluorescent signals in the root xylem of the transgenic seedlings (Fig. 4E), confirming the high accumulation of RD26 in the vasculature. Upon *R. solanacearum* inoculation, this fluorescent signal was decreased in the xylem of *proRD26:RD26-VENUS* roots (Fig. 4E), suggesting that RD26 is being degraded. To test whether the degradation of RD26 is dependent on FER, we introduced the *proRD26:RD26-VENUS* transgene into the *fer-4* mutant. The fluorescent signal only slightly decreased in *fer-4 proRD26:RD26-VENUS* roots after inoculation with *R. solanacearum* (Fig. 4E), indicating that RD26 is degraded in vivo in a FER-dependent manner.

We further detected RD26-VENUS with an anti-GFP antibody in the roots of *proRD26:RD26-VENUS* and *fer-4 proRD26:RD26-VENUS* seedlings. RD26 protein abundance decreased by 64% in *proRD26:RD26-VENUS* roots but only by 35% in *fer-4 proRD26:RD26-VENUS* roots following *R. solanacearum* inoculation (Fig. 4F), confirming the FER-dependent degradation of RD26 in planta. To determine if FER regulates the *RD26* transcript levels, we performed RT-qPCR in the

roots of Col-0 and *fer-4* seedlings. We observed no significant difference between Col-0 and *fer-4* (Supplementary Fig. S7F). Additionally, *R. solanacearum* infection showed no effect on *RD26* transcript levels in the roots of *proRD26:RD26-VENUS* or *fer-4 proRD26:RD26-VENUS* seedlings (Supplementary Fig. S7G). These results indicate that FER does not affect the transcript levels of *RD26* in roots. Based on these findings, we propose that FER interacts with RD26 and promotes the degradation of RD26 through phosphorylation.

RD26 positively regulates plant resistance to *R. solanacearum*

To investigate the biological function of RD26 during *R. solanacearum* infection, we generated *RD26*-overexpressing transgenic lines (*RD26*-OE #1 and *RD26*-OE #2) in Arabidopsis. These transgenic lines had smaller rosettes and shorter petioles than did Col-0 plants (Supplementary Fig. S8, A and B). Additionally, we obtained two T-DNA insertion mutant lines, *rd26-1* and *rd26-2*. Notably, loss of RD26 function did not affect the growth of Arabidopsis plants, as the rosettes of the two *rd26* mutants had the same size as that of Col-0 (Supplementary Fig. S8, A and B). We inoculated the roots of Col-0, *RD26*-OE, *and rd26* seedlings with *R. solanacearum* in vitro as previously described (Lu et al. 2018). Overexpression of *RD26* significantly decreased the suppression of root growth imposed by *R. solanacearum* infection, while *rd26-1* and *rd26-2* exhibited a greater suppression of root growth than did Col-0 (Fig. 5, A and B).

We also inoculated adult plants with the pathogen using the natural soil drenching method. The *RD26*-OE lines showed delayed wilting symptoms compared to Col-0, while *rd26-1* and *rd26-2* displayed accelerated disease development compared to Col-0 (Fig. 5, C and D). Next, we quantified the bacterial titers in the roots of Col-0, *RD26*-OE, and *rd26* seedlings following *R. solanacearum* inoculation. Starting at 4 days post inoculation (dpi), the *RD26*-OE lines had significantly lower bacterial counts than did Col-0, while the bacterial titer was higher in *rd26* than in Col-0 (Fig. 5E). These results indicate that RD26 plays a positive role in enhancing plant resistance to bacterial wilt. To investigate the role of the FER–RD26 cascade in plant resistance to *R. solanacearum*, we generated the *fer-4 rd26-1* double mutant and *RD26*-OE transgenic lines in the *fer-4* background (*fer-4 RD26*-OE) (Supplementary Fig. S8, C and D). Compared to *fer-4*, the elongation of *fer-4 RD26*-OE roots was not as suppressed by *R. solanacearum* infection, while that of *fer-4 rd26-1* roots was more sensitive to *R. solanacearum* infection (Fig. 5, F and G), indicating that RD26 functions downstream of FER.

In addition, we generated $RD26^{mutA}$-overexpressing transgenic lines in the *rd26-1* background (*rd26-1* $RD26^{mutA}$-OE). The roots of *rd26* $RD26^{mutA}$-OE seedlings were slightly but significantly longer than those of *RD26*-OE seedlings, indicative of decreased sensitivity to *R. solanacearum*-imposed suppression of root growth (Fig. 5, F and G). Taken together, these results suggest that RD26 functions downstream of FER and positively regulates plant resistance to bacterial wilt.

fer-4 and *RD26*-OE share a similar transcriptome profile and regulate the expression of lignin-related genes upon *R. solanacearum* infection

To investigate the relationship between the resistance phenotype of *RD26*-OE and *fer-4*, we conducted transcriptome deep sequencing (RNA-seq) analysis in the roots of *RD26*-OE, *fer-4*, and Col-0 without *R. solanacearum* inoculation. In *fer-4*, we identified 2,569 differentially expressed genes (*fer*-DEGs) compared to Col-0 ($P < 0.05$ and $|\log_2[\text{fold-change}]| > 1$). Similarly, we identified 1,794 DEGs in *RD26*-OE (*RD26*-OE-DEGs) compared to Col-0 ($P < 0.05$ and $|\log_2 FC| > 1$). There was a significant overlap between the DEGs detected for both comparisons (Supplementary Fig. S9A). Most of the DEGs exhibited consistent expression patterns in *fer-4* and *RD26*-OE roots, with a high degree of correlation ($R = 0.78$, $P < 0.001$) (Supplementary Fig. S9B). A gene ontology (GO) term enrichment analysis indicated that the DEGs shared by *fer-4* and *RD26*-OE are associated with various biological processes, including phytohormone signaling, dehydration, abiotic stimulus, hypoxia, and salt stress (Supplementary Fig. S9, C and D). We performed a similar RNA-seq analysis on the roots of *fer-4* and *RD26*-OE seedlings after *R. solanacearum* inoculation. The DEGs in response to *R. solanacearum* infection in the genotypes were again largely overlapping (Supplementary Fig. S10, A to C). The upregulated genes in *fer-4* and *RD26*-OE after *R. solanacearum* inoculation were enriched in cellular response to chemical stimuli, response to bacterium, and lignin metabolism (Supplementary Fig. S10, D and E). These findings support our earlier observation of increased cell wall lignification upon *R. solanacearum* inoculation (Fig. 1, B and C). Overall, the above gene expression analysis indicates that loss of FER function and *RD26* overexpression elicit similar transcriptional responses in the absence and presence of *R. solanacearum*.

Based on our transcriptome analysis, which revealed the upregulation of lignin-related genes in *fer-4* and *RD26*-OE after *R. solanacearum* infection (Supplementary Fig. S11A), we hypothesized that RD26 might regulate plant resistance to *R. solanacearum* by activating the expression of these genes. We searched for RD26-binding motifs in the promoters of lignin-related genes induced by *R. solanacearum*, based on the previously determined NAC recognition sequence containing CATGT and harboring CACG as the core DNA-binding sites (Tran et al. 2004). We identified RD26-binding motifs in the promoters of most lignin-related genes including *PAL1*, *MYB63*, and *MYB52* (Fig. 6A, Supplementary Fig. S11B). To validate the binding of RD26 to these promoters in vivo, we performed chromatin immunoprecipitation followed by quantitative PCR (ChIP-qPCR) using *35S:RD26-GFP* (*RD26*-OE) seedlings with an anti-GFP antibody. We detected the enrichment of DNA fragments from the *PAL1*, *MYB63*, and *MYB52* promoters among the immunoprecipitated chromatin in these *RD26*-OE seedlings, using Col-0 as a negative control (Fig. 6B). Using an electrophoretic mobility shift assay (EMSA), we confirmed the direct binding of recombinant purified GST-RD26 to probes containing the CATGT and CACG motifs in the *PAL1*, *MYB63*, and *MYB52* promoters (Fig. 6C, Supplementary Fig. S11C). Subsequently, we cloned the *PAL1*, *MYB63*, and *MYB52* promoters upstream of the *LUC* reporter gene and co-transfected each resulting reporter construct with a *35S:RD26* effector construct (or the empty vector as control) in Arabidopsis protoplasts. The presence of RD26 significantly increased relative luciferase activity compared to the empty vector control, indicating that RD26 activates transcription from the *PAL1*, *MYB63*, and *MYB52* promoters (Fig. 6D). Additionally, we examined the expression of these genes in the roots of Col-0, *RD26*-OE, *fer-4*, and *rd26* seedlings by RT-qPCR analysis. The overexpression of *RD26* or disruption of *FER* led to a significant upregulation of *PAL1*, *MYB63*, and *MYB52* expression, while knockout of *RD26* significantly downregulated the expression of these genes (Fig. 6, E to G). In summary, these results demonstrate that RD26 directly targets and regulates the expression of lignin-related genes.

RD26 regulates resistance to *R. solanacearum* in the xylem through lignin deposition

To investigate whether the FER–RD26 module specifically regulates lignin deposition in the root xylem, we stained lignin in the roots of

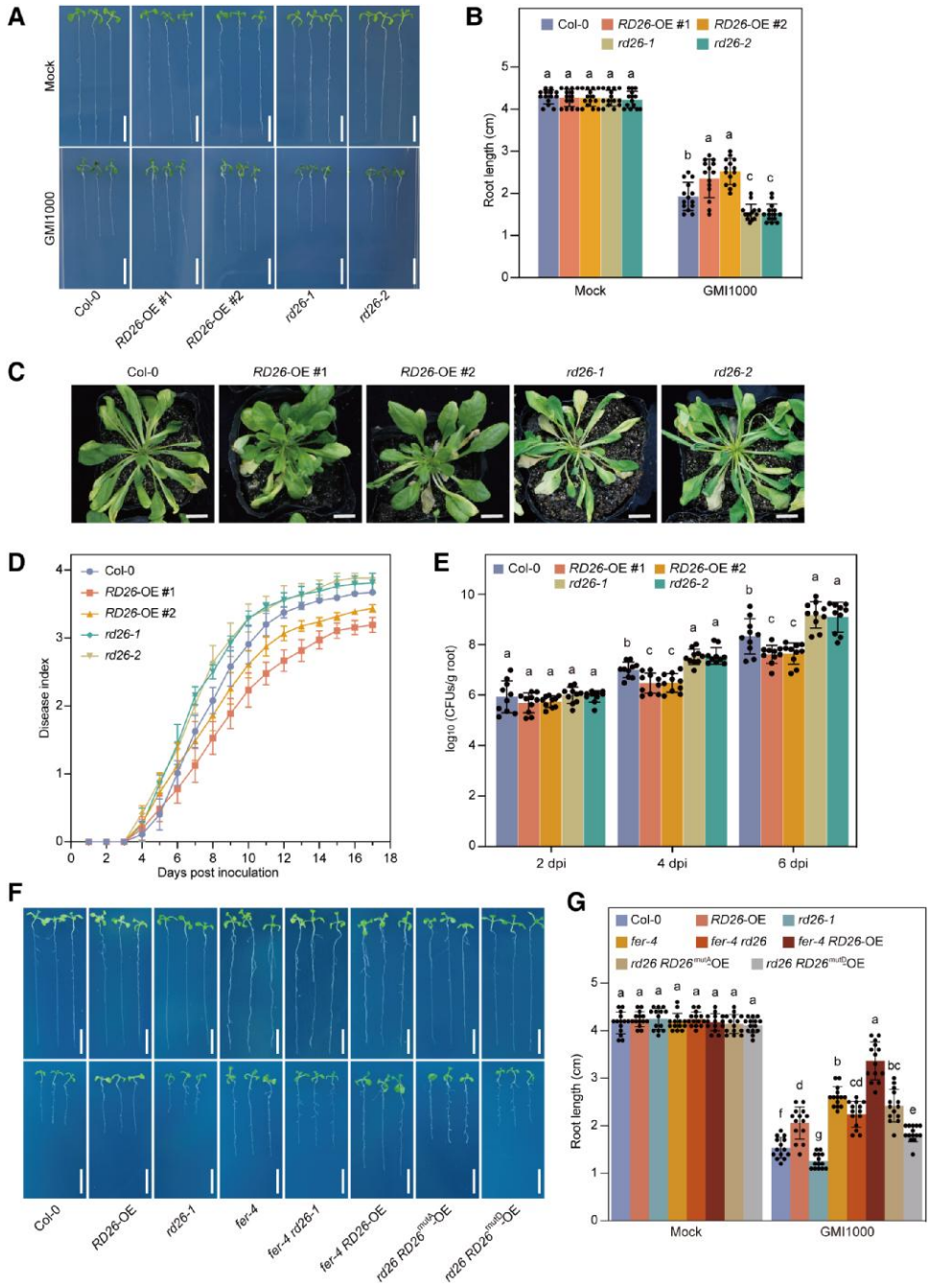

Figure 5. RD26 positively regulates plant resistance to *R. solanacearum*. **A** and **B)** Inoculation with *R. solanacearum* inhibits root growth of Arabidopsis seedlings. **A)** Seven-day-old seedlings of Col-0, *RD26*-OE (*RD26*-overexpressing transgenic lines), and *rd26* mutants were inoculated with 10 μL of a bacterial suspension at a titer of 1×10^7 CFUs/mL. The photographs were taken at 3 dpi. Scale bar, 1 cm. **B)** Root length of the seedlings shown in **(A)**. Values are means ± SD ($n=14$). Different lowercase letters indicate significant differences by one-way ANOVA ($P<0.05$). **C** and **D)** Bacterial wilt phenotype of Col-0, *RD26*-OE, and *rd26* plants after inoculation with *R. solanacearum*. Different Arabidopsis genotypes were inoculated with 20 mL of a bacterial suspension at a titer of 1×10^8 CFUs/mL. **C)** Representative photographs of infected plants showing the wilt phenotype. Photographs were taken at 8 dpi. Scale bar, 1 cm. **D)** Disease index of the inoculated plants, recorded daily. The average disease index is shown. The values represent means ± SD ($n=10$). **E)** Quantification of bacterial titer in Arabidopsis roots after *R. solanacearum* inoculation. The number of bacteria in the roots of Arabidopsis plants was determined at 2, 4, and 6 dpi. Values are means ± SD ($n=10$). Different lowercase letters indicate significant differences by one-way ANOVA ($P<0.05$). **F** and **G)** Inoculation with *R. solanacearum* inhibits root growth of Arabidopsis seedlings. **F)** Seven-day-old seedlings of Col-0, *RD26*-OE, *rd26-1*, *fer-4*, *fer-4 rd26-1*, *fer-4 RD26*-OE, *rd26 RD26*^{mutA}-OE, and *rd26 RD26*^{mutD}-OE were inoculated with a bacterial suspension at a titer of 10 μL of 1×10^7 CFUs/mL. The photographs were taken at 3 dpi. Scale bar, 1 cm. **G)** Root length of the seedlings shown in **(F)**. Values are means ± SD ($n=14$). Different lowercase letters indicate significant differences by one-way ANOVA ($P<0.05$). All experiments were performed 3 times with similar results.

Col-0, *RD26*-OE, and *rd26* seedlings with phloroglucinol-HCl. We determined that lignin specifically accumulates in the root xylem of *RD26*-OE seedlings (Fig. 7A), reflecting the precise regulation of lignin by RD26 in this tissue. Next, we quantified lignin levels in the roots of Col-0, *RD26*-OE, and *rd26* seedlings under normal growing conditions. The root xylem of *RD26*-OE seedlings had a higher lignin content than did that of Col-0, while mutation of *RD26* significantly decreased lignin content (Fig. 7B). We also assessed

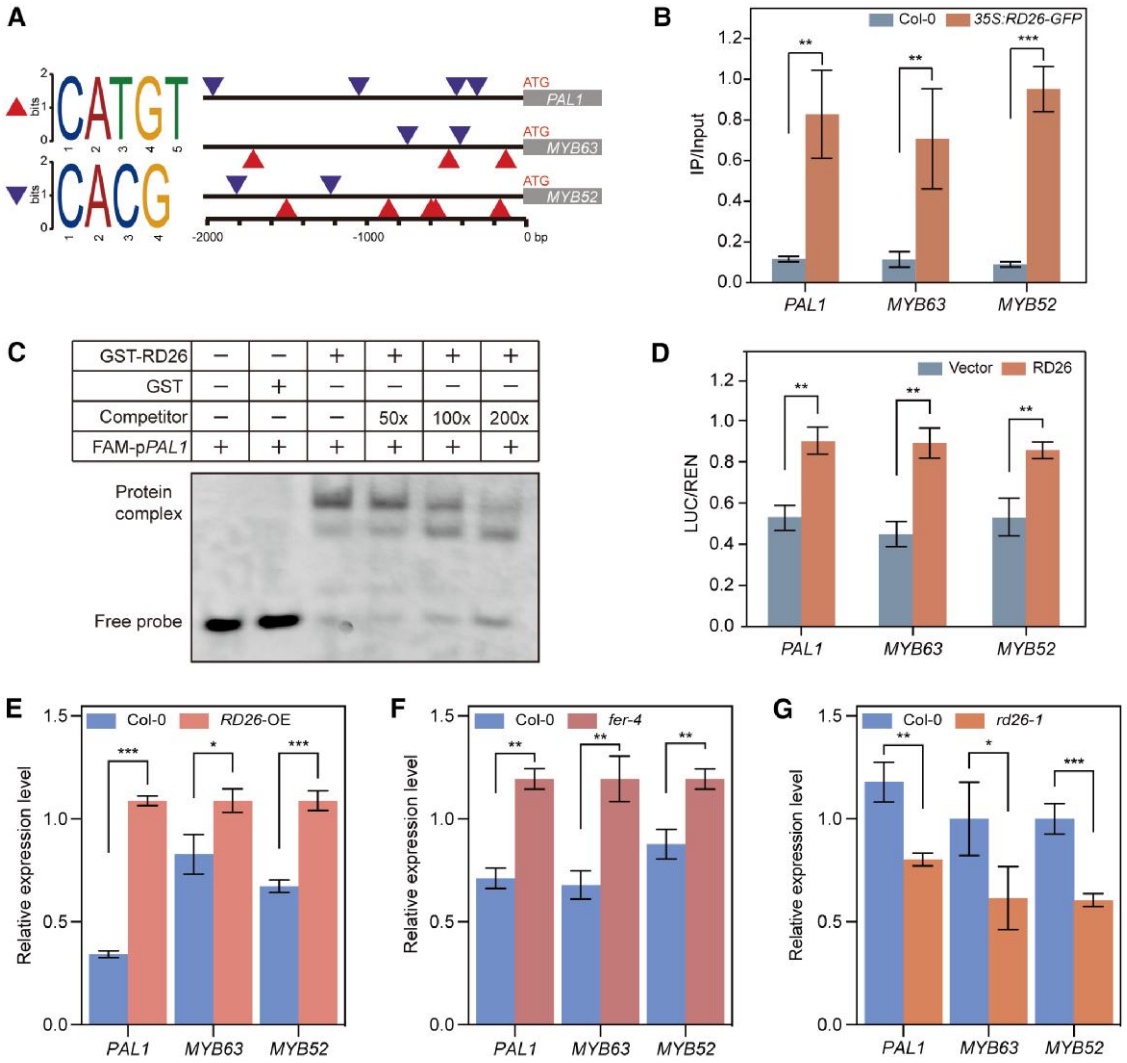

Figure 6. RD26 targets lignin-related genes. **A)** Prediction of RD26-binding sites (CATGT and CACG) within 2,000 bp of the *PAL1*, *MYB63*, and *MYB52* promoters. The positions are relative to the start codon. **B)** Chromatin immunoprecipitation quantitative PCR (ChIP-qPCR) assay showing that RD26 binds to the *PAL1*, *MYB63*, and *MYB52* promoters. Seven-day-old Arabidopsis seedlings of *35S:RD26-GFP* and Col-0 were used for the experiment, and anti-GFP was used for the IP. Values are means ± SD ($n = 3$). $^{**}P < 0.01$; $^{***}P < 0.001$ (Student's *t*-test). **C)** EMSA showing that recombinant purified GST-RD26 binds to a fragment of the promoter of the lignin-related gene *PAL1* in vitro. The probe is a FAM fluorescence-labeled DNA probe. Unlabeled probe was used as competitor. **D)** RD26 activates the promoters of lignin-related genes in planta. The promoters of the lignin-related genes were cloned upstream of the firefly *LUC* reporter gene. The resulting *promoter:LUC* constructs were co-transfected in Arabidopsis protoplasts together with the effector construct *35S:RD26* or the empty vector control. **E** to **G**) RT-qPCR analysis of relative transcript levels for the lignin-related genes *PAL1*, *MYB63*, and *MYB52* in *RD26*-OE (*RD26*-overexpressing transgenic line) and Col-0 (E), Col-0 and *fer*-4 (F), and Col-0 and *rd26* (G). **D–G)** Values are means ± SD ($n = 3$); $^{*}P < 0.05$; $^{**}P < 0.01$; $^{***}P < 0.001$ (Student's *t*-test). Experiments were performed 3 times with similar results.

pathogen-induced lignification by challenging Arabidopsis seedlings with *R. solanacearum*. The lignin content increased more prominently in *RD26*-OE seedlings than in *rd26* seedlings upon infection, relative to the mock control (Fig. 7, A and B). We also observed the induction of lignin deposition in *rd26* in response to *R. solanacearum* (*rd26*, GMI1000 vs. Mock) (Fig. 7, A and B), suggesting that plants employ alternative pathways, in addition to RD26, to regulate lignin biosynthesis in response to *R. solanacearum* infection.

Next, we determined the lignin content in the roots of *fer*-4 *RD26*-OE and *fer*-4 *rd26*-1 seedlings. After inoculation with *R. solanacearum*, the lignin content of *fer*-4 *rd26*-1 was clearly lower than that in *fer*-4, while the lignin content of *fer*-4 *RD26*-OE was higher than that in *fer*-4 (Supplementary Fig. S12), confirming that RD26 functions downstream of FER. Furthermore, we examined bacterial colonization in the roots of Col-0, *RD26*-OE, and *rd26* seedlings. *Ralstonia solanacearum* showed a diminished colonization of the root xylem of *RD26*-OE seedlings compared to Col-0, while the bacteria proliferated more in the roots of *rd26* seedlings (Fig. 7C). These results suggest that RD26-mediated regulation of lignin in the root xylem confers resistance to *R. solanacearum*.

To further elucidate the role of RD26 in xylem resistance to *R. solanacearum*, we assessed lignin deposition and bacterial colonization in the roots of the transgenic line expressing *RD26* specifically in the xylem from the *MGT6* promoter (Supplementary Fig. S5). Upon *R. solanacearum* inoculation, the RD26-VENUS signal in the parenchyma tissue decreased substantially (Fig. 7D), suggesting RD26 degradation. When we analyzed lignin levels in the roots of Col-0, *rd26*, and *rd26 proMGT6:RD26-VENUS* seedlings, we observed a comparable lignin accumulation in Col-0 and *rd26 proMGT6:RD26-VENUS*, whereas lignin deposition was significantly lower in *rd26* (Fig. 7, E and F). We also evaluated bacterial colonization in the roots of Col-0, *rd26*, and *rd26 proMGT6:RD26-VENUS* seedlings. *Ralstonia*

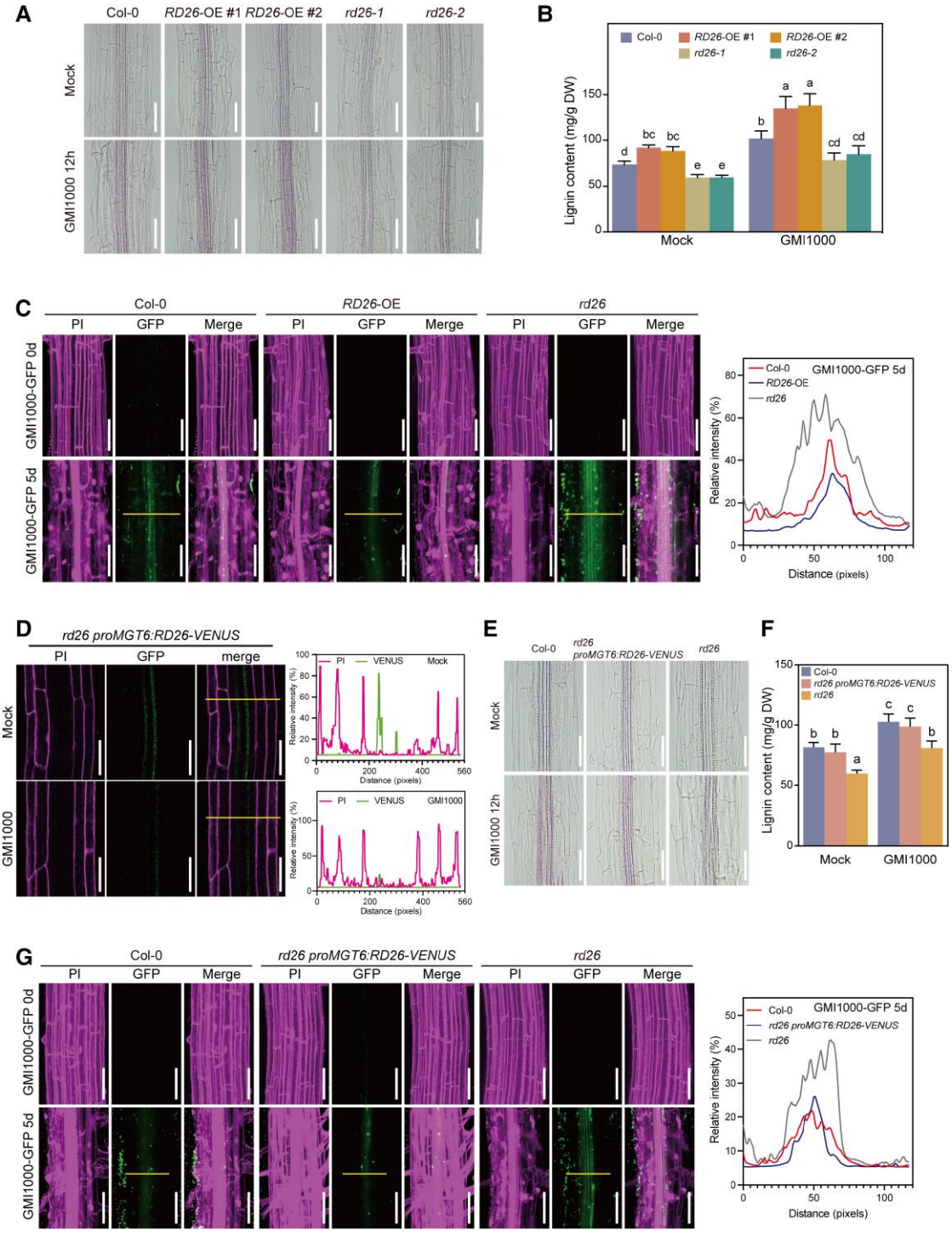

Figure 7. RD26 regulates resistance to *R. solanacearum* in the xylem through lignin deposition. **A** and **B)** Lignin visualization **(A)** and quantification **(B)** in xylem of Arabidopsis roots at 12 hpi with *R. solanacearum*. Roots from Col-0, *RD26*-OE (*RD26*-overexpressing transgenic lines), and *rd26* Arabidopsis seedlings were stained with phloroglucinol-hydrochloric acid (HCl). Scale bars, 50 μm. DW, dry weight (oven drying). Values are means ± SD ($n = 3$). Different lowercase letters indicate significant differences by one-way ANOVA ($P < 0.05$). **C)** Differential colonization of *R. solanacearum* in Col-0, *RD26*-OE, and *rd26* roots. Seven-day-old seedlings were inoculated with GMI1000-*GFP* at a titer of 10 μL of 1×10^7 CFUs/mL. Green represents GFP signals. Magenta indicates PI staining of the cell walls. Scale bars, 50 μm. Quantification of GFP fluorescence signal along the yellow lines after inoculation with *R. solanacearum* is shown to the right. **D)** Spatial expression pattern of *proMGT6:RD26* in *rd26 proMGT6:RD26-VENUS* seedlings in response to *R. solanacearum* inoculation. The *rd26 proMGT6:RD26-VENUS* reporter line was inoculated with GMI1000 at a titer of 10 μL of 1×10^7 CFUs/mL. Confocal microscopy images were captured at 12 hpi. Green represents VENUS signals. Magenta indicates PI staining of the cell walls. Scale bars, 50 μm. Quantification of fluorescence signal along the yellow lines in the *rd26 proMGT6:RD26-VENUS* reporter line after inoculation with *R. solanacearum* is shown to the right. **E** and **F)** Lignin visualization **(E)** and quantification **(F)** in the xylem of roots from Arabidopsis Col-0, *rd26 proMGT6:RD26-VENUS* and *rd26* seedlings. Roots were stained with phloroglucinol-HCl. Scale bars, 50 μm. Values are means ± SD ($n = 3$). Different lowercase letters indicate significant differences by one-way ANOVA ($P < 0.05$). **G)** Differential colonization of *R. solanacearum* in the roots of Col-0, *rd26 proMGT6:RD26-VENUS*, and *rd26* seedlings. Seven-day-old seedlings were inoculated with GMI1000-*GFP* at a titer of 10 μL of 1×10^7 CFUs/mL. Green represents GFP signals. Magenta indicates PI staining of the cell walls. Scale bars, 50 μm. Quantification of GFP fluorescence signal along the yellow lines after inoculation with *R. solanacearum* is shown to the right. Experiments were performed 3 times with similar results.

solanacearum colonization levels were comparable in Col-0 and *rd26 proMGT6:RD26-VENUS*, both of which were lower than in *rd26* (Fig. 7G). These results suggest that the tissue-specific expression of *RD26* in parenchyma cells rescues lignin deposition and bacterial colonization in the xylem.

To confirm the role of xylem lignin in plant resistance to *R. solanacearum*, we assessed the extent of xylem lignification and bacterial wilt phenotype of *ccoaomt1*, a mutant in *CAFFEOYL COENZYME A O-METHYLTRANSFERASE 1* defective in lignin biosynthesis (Do et al. 2007). Phloroglucinol-HCl staining showed that lignin accumulates to lower levels in the root xylem of *ccoaomt1* seedlings than in that of Col-0 (Supplementary Fig. S13A), confirming the role of CCoAOMT1 in lignin biosynthesis. Next, we examined bacterial colonization in the roots of Col-0 and *ccoaomt1* seedlings. *Ralstonia solanacearum* colonized more of the root xylem in *ccoaomt1* seedlings than in Col-0 seedlings (Supplementary Fig. S13B), validating the role of xylem lignin in plant resistance to the vascular bacterial pathogen *R. solanacearum*. Further in vitro and natural soil drench inoculation assays also confirmed the susceptible phenotype of *ccoaomt1* against *R. solanacearum* (Supplementary Fig. S13, C to F).

The FER–RD26 module regulates lignin biosynthesis and resistance to *R. solanacearum* in tomato and tobacco (*Nicotiana tabacum*)

Ralstonia solanacearum has a wide host range, with Solanaceae plants such as tomato being the most common hosts. To explore the function of FER and RD26 in resistance to *R. solanacearum* in tomato, we used RNA interference (RNAi) to silence *SlFER* (Solyc09g015830) or *SlRD26* (Solyc12g013620, also reported as *SlJA2*). RT-qPCR analysis revealed the significant decrease in *SlFER* or *SlRD26* transcript levels in silenced lines (Supplementary Fig. S14A). Next, we evaluated lignin deposition in the roots of these *SlFER*-RNAi and *SlRD26*-RNAi seedlings. Based on phloroglucinol-HCl staining, lignin accumulated to a higher level in *SlFER*-RNAi roots, while it accumulated less in *SlRD26*-RNAi roots, than in seedlings of a line transformed with the empty vector (EV) as control (Fig. 8A). Quantification of lignin levels also confirmed the negative role of SlFER and the positive role of SlRD26 in lignin accumulation (Fig. 8B). We inoculated EV, *SlFER*-RNAi, and *SlRD26*-RNAi seedlings with *R. solanacearum*. Silencing of *SlFER* enhanced tomato resistance to *R. solanacearum*, while silencing of *SlRD26* promoted *R. solanacearum* infection (Fig. 8, C to E). These results demonstrate the similar role of FER and RD26 in plant lignin biosynthesis and resistance to *R. solanacearum* in tomato and Arabidopsis.

To assess the negative role of FER in bacterial wilt resistance in tobacco (*Nicotiana tabacum*), we evaluated the disease phenotype of *Ntfer* mutants in one of the two tobacco *FER* genes, previously generated in our laboratory via clustered regularly interspaced short palindromic repeats (CRISPR)/CRISPR-associated nuclease 9 (Cas9)-mediated gene editing (Supplementary Fig. S14B). Compared to wild-type plants (K326), *Ntfer* mutants showed delayed disease progression and diminished bacterial colonization (Supplementary Fig. S14, C to E), although the resistance phenotype of *Ntfer* was not as pronounced as that seen in the *fer-4* mutant of Arabidopsis, possibly because the tobacco genome harbors two copies of *FER*, which might redundantly mediate resistance to *R. solanacearum*. In addition, phloroglucinol-HCl staining and quantification of lignin content confirmed that the *Ntfer* mutant has a higher lignin content than its corresponding wild type (Supplementary Fig. S14, F and G).

We showed above that RD26 targets lignin-related genes such as *PAL1*, *MYB63*, and *MYB52* (Fig. 6 and Supplementary Fig. S11). To investigate the role of these RD26 target genes in lignin biosynthesis and resistance to *R. solanacearum*, we silenced *SlMYB115* (Solyc04g064540), the ortholog of *MYB52* in tomato (Supplementary Fig. S15A). Compared to the EV control, silencing of *SlMYB115* decreased lignin accumulation in tomato roots (Supplementary Fig. S15, B and C). We further inoculated EV and *SlMYB115*-RNAi plants with *R. solanacearum*. Silencing of *SlMYB115* diminished tomato resistance to *R. solanacearum* (Supplementary Fig. S14, D to F). These results indicate that the target genes of RD26 are also involved in lignin biosynthesis and resistance to *R. solanacearum* in tomato. To further demonstrate the role of xylem lignin in resistance to *R. solanacearum*, we silenced the homolog of *CCoAOMT1* in tomato, which we showed above negatively regulated lignin biosynthesis and resistance to *R. solanacearum* in Arabidopsis (Supplementary Fig. S13). The silencing of *SlCCoAOMT* decreased the lignin content of tomato roots and diminished resistance to *R. solanacearum* (Supplementary Fig. S15). Taken together, these results suggest that the FER–RD26 module regulates resistance to *R. solanacearum* through lignin accumulation in the root xylem in its natural hosts tomato and tobacco.

Discussion

Pathogens have developed unique genes or virulence strategies for successful infection of different plant tissues. For instance, the hydrolase gene *CbsA* in the family Xanthomonadaceae plays a key role in the phenotypic switch between vascular and nonvascular pathogens (Gluck-Thaler et al. 2020). However, the precise regulation of vascular-specific defense responses in plants against pathogens remains largely unknown. In this study, we discovered FER–RD26 as a module that governs plant vascular resistance to *R. solanacearum* in the xylem of Arabidopsis roots (Fig. 9). The FER–RD26 pathway represents a previously undescribed signaling pathway that maintains a balance between plant defense against the vascular pathogen *R. solanacearum* and the regulation of lignin in the root xylem. In a recent study by Lin et al., the MKP1–MAPK–MYB signaling cascade was revealed to regulate resistance to the vascular pathogen *Xanthomonas oryzae* pv. *oryzae* through lignin deposition (Lin et al. 2022). Together with this recent study, our work highlights the important role of lignin in root xylem for the regulation of plant resistance to vascular pathogens.

FER positively regulates plant immunity against *P. syringae* in leaves (Stegmann et al. 2017). However, in the roots, FER and its homolog in soybean (*Glycine max*) are exploited by rapid alkalinization factor (RALF)-like peptides from plant parasitic nematodes, acting as negative regulators of immunity against nematodes (Zhang et al. 2020a, 2021). Our previous work demonstrated that *FER* disruption or inhibition of FER-kinase activity enhanced plant resistance to *R. solanacearum* (Liu et al. 2023b), indicating that FER also acts as a negative regulator of plant immunity against this pathogen in roots. Notably, the genome of *R. solanacearum* does not encode putative RALF-like genes (Salanoubat et al. 2002), suggesting that FER, as the receptor of RALFs, is unlikely to be directly exploited by *R. solanacearum*. Instead, we reveal that FER phosphorylates and degrades the transcription factor RD26, resulting in decreased lignin biosynthesis and increased susceptibility to *R. solanacearum*. Similarly, FER can phosphorylate and destabilize the transcription factor MYC2, thereby regulating immunity against *P. syringae* (Guo et al. 2018; Wang et al. 2022). A recent study revealed that FER in tomato interacts with and degrades a MYB transcription factor to regulate lignin biosynthesis and resistance to *Fusarium oxysporum* f. sp. *lycopersici* (Fan et al. 2024). Hence, distinct mechanisms have evolved to enable FER to either

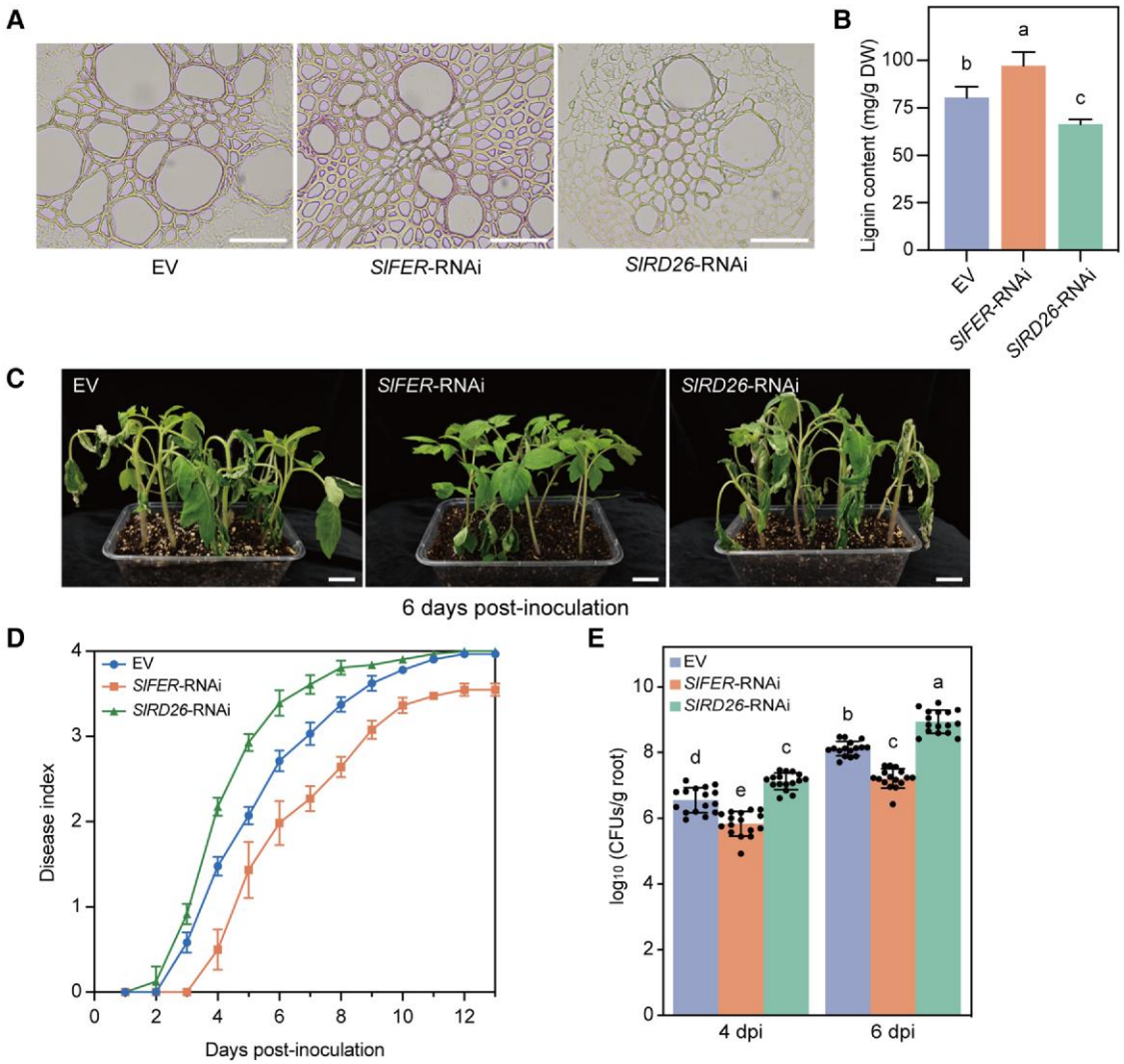

Figure 8. The FER–RD26 module regulates lignin biosynthesis and resistance to *R. solanacearum* in tomato. **A** and **B)** Lignin visualization **(A)** and quantification **(B)** in the roots of tomato seedlings silenced for *SlFER* or *SlRD26*. Roots were stained with phloroglucinol-hydrochloric acid (HCl). Scale bars, 50 μm. DW, dry weight (oven drying). Values are means ± SD ($n = 3$). Different lowercase letters indicate significant differences by one-way ANOVA ($P < 0.05$). **C** to **E)** Disease phenotype of *SlFER*-RNAi and *SlRD26*-RNAi tomato plants following *R. solanacearum* inoculation. **C)** Bacterial wilt disease phenotype of *SlFER*-RNAi and *SlRD26*-RNAi plants after inoculation with *R. solanacearum*. Plants were inoculated with 10 mL of a bacterial suspension at $OD_{600} = 0.1$. Photographs were taken at 6 dpi. Scale bar, 2 cm. **D)** Disease index of inoculated plants were recorded daily. The average disease index is shown. Values represent means ± SD ($n = 16$). **E)** Quantification of bacterial titer in tomato roots after *R. solanacearum* inoculation. The number of bacteria in the roots of tomato plants was determined at 4 and 6 dpi. Values are means ± SD ($n = 16$). Different lowercase letters indicate significant differences by one-way ANOVA ($P < 0.05$). Experiments were performed 3 times with similar results.

positively or negatively regulate plant immunity against different pathogens, even within the same plant tissue.

Our findings demonstrate that the FER–RD26 pathway regulates lignin deposition in the root xylem, which in turn controls *R. solanacearum* colonization and resistance to this pathogen. Consistent with our observations, several studies have shown that increased lignin content and greater lignification of cell walls occur following infection, together with resistance to vascular pathogens such as *Verticillium dahlia* (Ferreira et al. 2017; Li et al. 2019; Kashyap et al. 2021). Despite the diverse functions of lignin in plant defense regulation, the mechanisms by which cell wall lignification in the xylem enhances plant resistance to *R. solanacearum* are yet to be fully characterized. One possibility is that *fer-4*-regulated lignification acts as a physical barrier, impeding the movement of *R. solanacearum* within the root xylem. *Ralstonia solanacearum* colonizing the xylem expresses genes encoding the type III secretion system and most of its associated effectors (Jacobs et al. 2012; Monteiro et al. 2012; de Pedro-Jové et al. 2021), which manipulate plant physiology, including immunity, to the benefit of the pathogen. Enhanced lignification of cell walls may hinder the injection of such effectors into target plant cells, thereby decreasing the virulence of *R. solanacearum* and indirectly enhancing plant resistance to this pathogen.

Our results indicate that FER acts as a negative regulator of lignin biosynthesis by promoting RD26 degradation during *R. solanacearum* infection. The increased expression of *FER* and decreased expression of *RD26* in the root xylem upon infection support this conclusion (Figs. 2A and 4E). However, one might wonder why the root xylem of Col-0 seedlings, where RD26 is theoretically degraded by FER, still accumulates higher levels of lignin after *R. solanacearum* infection (Fig. 1B). Lignin biosynthesis is governed by a complex regulatory network and is typically co-regulated by different pathways (Xie et al. 2018; Xu et al. 2022) and FER–RD26 represents only one regulatory pathway of lignin biosynthesis (Nakano et al. 2015). Thus, other

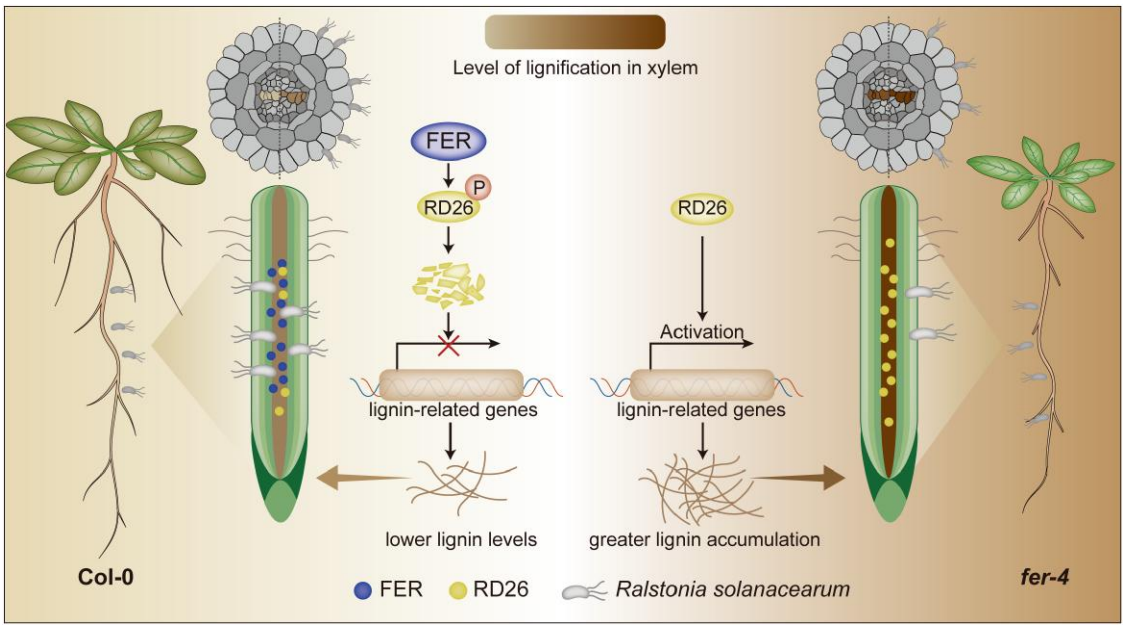

Figure 9. Conceptual model illustrating how FER–RD26 module regulates plant resistance to the vascular pathogen *R. solanacearum* through lignin biosynthesis. In Col-0 (left), FER accumulation is specifically induced in the xylem of roots upon *R. solanacearum* infection. FER phosphorylates and degrades RD26, a transcription factor that controls lignin biosynthesis, negatively regulating lignin content in the xylem, leading to greater *R. solanacearum* colonization of the root xylem and susceptibility to bacterial wilt. In *fer-4* (right), FER is not functional and cannot degrade RD26. The stable RD26 increases lignin content in the root xylem and results in enhanced resistance to *R. solanacearum*.

pathways can contribute to lignin production during *R. solanacearum* infection, as indicated by the significant lignin accumulation seen in *rd26* mutants after *R. solanacearum* infection (Fig. 7A). Excessive lignin accumulation can have a negative influence on plant growth and development (Zhong et al. 2006; Zhou et al. 2009), as also indirectly indicated by the growth phenotype of *RD26*-OE lines (Supplementary Fig. S8). Therefore, plants need to finely tune this trade-off between defense and growth. FER was shown to be involved in sensing cell wall integrity (Feng et al. 2018). We hypothesize that FER detects the boost of lignin deposition during *R. solanacearum* infection and degrades RD26 to partially restrict lignin biosynthesis, thereby maintaining a balance between plant defense and growth. As another means to achieve an optimal immune response while maintaining normal growth, plants trigger local immune responses at the site of infection or colonization. This strategy is also the most efficient and cost-effective for plant resistance to pathogens. In the case of roots, immune responses are differentially and precisely controlled in various cell types and developmental regions (Chuberre et al. 2018; Rich-Griffin et al. 2020; Zhou et al. 2020). Our discovery of FER–RD26-regulated lignification in the vascular xylem provides evidence of infection site-specific immune regulation and opens the door to identifying other signaling pathways or regulators that govern localized immunity. Understanding how different cell types or tissues in plants perceive invading pathogens and activate tissue- and infection-specific immunity may have broad implications for the development of plants resistant to various devastating pathogens.

Materials and methods

Plant materials and growth conditions

For the generation of *35S:RD26-GFP* (*RD26*-OE), *35S:RD26-MYC* (*RD26*-OE), *35S:RD26^{mutA}-GFP*, and *35S:RD26^{mutD}-GFP* transgenic Arabidopsis (*A. thaliana*), full-length coding sequences of *RD26*, *RD26^{mutA}*, and *RD26^{mutD}* fused with a C-terminal GFP/MYC tag under the control of the 35S promoter was cloned into pDT1 as previously described (Zhu et al. 2020). For the generation of *proRD26:RD26-VENUS* transgenic Arabidopsis, full-length coding sequences of *RD26* fused with a C-terminal VENUS tag driven by the RD26 promoter was cloned into p1300-LV. For the generation of *proMGT6:RD26-VENUS* transgenic Arabidopsis, full-length coding sequences of *RD26* fused with a C-terminal VENUS tag driven by the MGT6 promoter was cloned into p1300-LV. Transgenic plants were obtained by transforming the plasmid into WT Columbia (Col-0) background with *Agrobacterium*-mediated transformation. The *rd26-1* (SALK_063576C) T-DNA insertion mutant and *ccoaomt1* (SALK_055103C) T-DNA insertion mutant were obtained from the AraShare (https://www.arashare.cn/index/). The *rd26-2* (SALK_083756) mutant was kindly provided by Dr. Xiaoyun Li. Homozygosity of mutants was identified by PCR (Supplementary Table S1). *fer-4* and *proFER:FER-GFP* were as previously described (Duan et al. 2010). The *proPAL1:PAL1-VENUS* were kindly provided by Jingshi Xue and Laigeng Li. Multiple mutants are generated by crossing individual lines, usually with *fer-4* as the female parent. Seeds of Arabidopsis were first sterilized with 75% [v/v] ethanol for 5 min, followed by treatment with 15% [v/v] sodium hypochlorite for 5 min. The seeds were washed with sterile water and sown on half-strength Murashige and Skoog (MS) medium. Arabidopsis seedlings were grown in a growth chamber at 22 °C with 10 h/14 h light/dark cycle.

The tobacco (*Nicotiana tabacum*) FER mutant *Ntfer* was generated by CRISPR-Cas9. Briefly, two gRNAs (gRNA1: GTCTGAGTTCA CCTATAGTT; gRNA2: CCAATGCCATTTTCGGTGTG) were designed to target the coding sequence of NtFER and cloned into the binary vector p201. The CRISPR-Cas9 construct was transformed into wild-type tobacco (cv. K326) via *Agrobacterium* GV3101. The mutation was confirmed by Sanger sequencing.

Yeast two-hybrid assay

The yeast two-hybrid (Y2H) assay was performed as previously described (Yu et al. 2012). Briefly, the kinase domain of *Cr*RLK1Ls

was amplified by PCR with specific primers (Supplementary Table S1) and fused in-frame with the GAL4 DNA-binding domain of the bait vector pGBKT7 (BD-CrRLK1Ls). The coding sequence (CDS) of full-length *RD26* was fused with the GAL4 DNA-activating domain of the prey vector pGADT7 (AD-RD26). Distinct plasmid pairs were transformed into yeast AH109 cells. The diluted transformants were plated onto synthetic dropout medium lacking tryptophan/leucine (SD/-Trp-Leu+His) and synthetic dropout medium lacking tryptophan/leucine/histidine (SD/-Trp-Leu-His) but supplemented with 3-amino-1,2,4-triazole (3-AT) for 4 days to test the interaction.

Pull-down assay

The full-length *RD26* CDS was cloned into the pGEX-4T-1 and transformed into *E. coli* BL21 to express a GST-RD26 fusion protein at 16 °C. GST-tagged RD26 proteins were purified according to manufacturer's manual using Pierce Glutathione Agarose (16102, Thermo Fisher Scientific, USA). The 6× His-tagged FER-KD were purified as previously described (Chen et al. 2016). Recombinant FER-KD protein was incubated overnight at 4 °C with GST beads coupled with GST-RD26 in the binding buffer (50 mM Tris-HCl [pH = 7.5], 150 mM NaCl, 5 mM $MgCl_2$). Then, the beads were washed 3 times with the washing buffer (50 mM Tris-HCl [pH = 7.5], 150 mM NaCl, 0.1% [v/v] Triton X-100) and boiled the beads in sodium dodecyl sulfate polyacrylamide gel electrophoresis (SDS-PAGE) loading buffer, and eluted proteins were analyzed by immunoblotting with anti-His (M20001, Abmart) or anti-GST (SC-80998, CMC) antibody.

LCI assay

Firefly Luciferase complementation imaging assays were performed as previously described (Chen et al. 2008). In brief, the cDNA of indicated genes were amplified and cloned into 35S-pCAMBIA1300-Nluc or 35S-pCAMBIA1300-Cluc. The *A. tumefaciens* strain GV3101 carrying these plasmids was co-infiltrated into *N. benthamiana* leaves. After cultivating in the dark for 48 h, the reaction substrate D-luciferin (Biovision, Cat No.7903) was applied, and the luminescence images were captured using a CCD imaging system to determine the interaction between proteins.

Co-IP assay

Co-IP was performed as previously described with some modifications (Du et al. 2016). Seven-day-old seedlings *35S:RD26-GFP* (about 0.5 g) were ground to a fine powder in liquid nitrogen and solubilized with 500 μL NEB-T buffer (20 mM HEPES [pH = 7.5], 40 mM KCl, 5 mM $MgCl_2$, 0.1% [v/v] Triton X-100) containing 1× protease inhibitor cocktail (78430, Thermo Fisher Scientific) and 1× phosphatase inhibitor (78420, Thermo Fisher Scientific) for 1 h on ice. The extracts were centrifuged at 16,000 × *g* at for 10 min at 4 °C, and the supernatant was transferred to incubate with prepared 20 μL Protein A/G magnetic beads (B23202), which had been preincubated with anti-FER for several hours. They were gently shaked together at 4 °C overnight, and 100 μL supernatant was used as input. Then, the beads were washed 3 times with the NEB-T buffer. Anti-FER (Du et al. 2016) and anti-GFP (CST, 55494S) antibody were used for detection of FER and RD26, respectively.

In vitro phosphorylation assay and LC-MS/MS analysis

The purity of recombinant GST-RD26, GST-RD26^{mutA} and His-FER-KD/His-FER^{K565R}-KD (kinase-dead form) proteins (Xu et al. 2024) was assessed by SDS-PAGE. One microgram recombinant proteins (GST-RD26/GST-RD26^{mutA} and His-FER-KD/His-FER^{K565R}-KD) were mixed and added to the reaction buffer (50 mM Tris-HCl [pH = 7.5], 10 mM $MgCl_2$, 1 mM $CaCl_2$, 1 mM ATP, 1 mM DTT) in a total volume of 50 μL. After gentle mixing, the mixture was incubated at 25 °C for 30 min. The reaction was stopped by adding 2× SDS loading buffer. Proteins were separated on a 10% SDS-PAGE gel and detected with Anti-Phosphoserine antibody and Anti-Phosphothreonine antibody (p-Ser, Abcam ab9332; p-Thr, Abcam ab9337). LC-MS/MS analysis was performed by Shanghai Bioprofile Technology (Shanghai, China). Mass spectrometry was performed by LC-MS/MS as described previously (Du et al. 2016). The mass spectrometry database search software used in this project is MaxQuant (version 1.6.17.0). The criteria used for filtering peptide, modification site, and protein identifications after mass spectrometry data search are as follows: PSM FDR < 0.01, Site FDR < 0.01, Protein FDR < 0.01.

In vivo phosphorylation assay

Seven-day-old seedlings of *35S:RD26-MYC*, *fer-4 35S:RD26-MYC*, and Col-0 (about 0.5 g) were ground into a fine powder in liquid nitrogen and solubilized with 500 μL NEB-T buffer containing 1× protease inhibitor cocktail (78430, Thermo Fisher Scientific) and 1× phosphatase inhibitor (78420, Thermo Fisher Scientific) for 1 h on ice. Then, the extracts were centrifuged at 16,000 × *g* at for 10 min at 4 °C, and the supernatant was transferred to incubate with prepared 20 μL Anti-MYC magnetic beads (P2118) overnight at 4 °C with gentle shaking, and 100 μL supernatant was used as input. For the detection of phosphorylated RD26 proteins, 20 μL sample was separated by 10% SDS-PAGE. Blots were probed with p-Ser/p-Thr antibody (p-Ser, Abcam ab9332; p-Thr, Abcam ab9337) or MYC antibody (CST, 9405S).

Cell-free degradation assay

Seven-day-old seedlings (approximately 0.3 g) were ground into a fine powder in liquid nitrogen and then dissolved in 500 μL of cell-free degradation buffer (25 mM Tris-HCl [pH = 7.5], 10 mM NaCl, 10 mM $MgCl_2$, 1 mM ATP, 5 mM DTT). This mixture was incubated on ice for 1 h. Subsequently, the extracts were subjected to centrifugation at 16,000 × *g* for 10 min at 4 °C. The resulting supernatant was then combined with 1 mg of the prepared fusion protein and allowed to react at room temperature. Samples were collected at 0, 15, 30, 45, and 60 min. As a control, a sample containing MG132 was used. Protein analysis was performed through immunoblotting using an anti-GST antibody (SC-80998, CMC). Coomassie Brilliant Blue G250 staining (CBB) was employed to assess and normalize protein loading.

Protein half-life determination

This assay was carried out as described with modifications (Guo et al. 2018). Briefly, Arabidopsis seeds were germinated on half-strength MS medium plates vertically for 7-day-old. Seedlings were transferred to half-strength MS liquid medium with 50 mM MG132, and gently shaken for 16 h, and then 1 mL half-strength MS liquid medium containing 400 mM CHX or DMSO control was added so the final CHX concentration is 200 μM. Seedlings were collected and gently dabbed dry and flash frozen in liquid nitrogen. The samples were ground in 2× SDS sample buffer and used for western blotting. Protein half-life was estimated as the time when the protein level decreased to half of the amount of the control.

Transient expression of RD26 in Col-0 and *fer-4* Arabidopsis leaves

Agrobacterium-mediated transient transformation of Arabidopsis was performed according to a previously described method (Zhang et al. 2020c). The constructs were transformed into *A. tumefaciens* AGL1 strain. The agrobacterial cells were harvested and washed with washing solution (10 mM $MgCl_2$ and 100 μM Acetosyringone). After the agrobacteria solution was diluted to OD_{600} of 0.5 with the infiltration solution (quarter-strength MS [pH = 6.0], 1% [w/v] sucrose, 100 μM Acetosyringone, 0.01% [v/v] Silwet L-77). The agrobacteria solution was infiltrated into the leaves of 4-week-old Arabidopsis. The plants were placed in the dark for 24 h and then transferred back to the growth chamber with light for another 2 to 3 days. The samples were ground in 2× SDS sample buffer and used for western blotting.

RNA isolation and RT-qPCR

Seven-day-old seedlings (about 0.2 g) were powdered in liquid nitrogen, then the RNA was extracted by TRIzol reagent (Ambion, 15596-026). First-strand cDNA was synthesized by using a cDNA synthesis kit (Fermentas, K1622), according to the manufacturer's instructions. qPCR was performed using the CFX96 Touch Real-Time PCR Detection System (Bio-Rad) with SYBR Premix *Ex*TaqII (Takara). Primers for RT-qPCR is shown in Supplementary Table S1. *ACTIN7* was used as a reference in qPCR analysis (Supplementary Table S1).

RNAi in tomato roots

To generate the *SlFER*-RNAi, *SlRD26*-RNAi, *SlCCoAOMT*-RNAi, and *SlMYB115*-RNAi constructs, fragments of the tomato genes *SlFER* (Solyc09g015830), *SlRD26* (Solyc12G013620), *SlCCoAOMT* (Solyc10g050160), and *SlMYB115* (Solyc04g064540) were amplified from tomato cDNA using the primers listed in Supplementary Table S1. These fragments were first cloned into pENTR-CACC-AAGG and then transferred into the expression vector pK7GWIWG2_II-RedRoot. The pK7GWIWG2_II-RedRoot vectors containing the target sequence were them transformed into the *Agrobacterium rhizogenes* MSU440 (Wang et al. 2021).

RNAi was performed as previously described (Wang et al. 2021). Briefly, the radicles of tomato seedlings were cut, and the resulting hypocotyls were dipped in *A. rhizogenes* MSU440 containing either pK7GWIWG2_II-RedRoot::*SlFER*, pK7GWIWG2_II-RedRoot::*SlRD26*, pK7GWIWG2_II-RedRoot::*SlCCoAOMT*, pK7GWIWG2_II-RedRoot::*SlMYB115*, or pK7GWIWG2_II-RedRoot as a control. The seedlings were then incubated to allow the growth of transgenic roots. Three weeks after transformation, the seedlings were transferred to soil. The silencing efficiency of the *SlFER*, *SlRD26*, *SlCCoAOMT*, and *SlMYB115* were determined by quantitative RT-PCR.

Inoculation assay

The *R. solanacearum* phylotype I strain GMI1000 and its derivative GMI1000-*GFP* were used for all *R. solanacearum* inoculations except for tobacco inoculations, for which the CQPS-1 strain was used because GMI1000 is avirulent toward tobacco owing to the presence of two Type III effectors (Poueymiro et al. 2009). After an overnight incubation in B medium (1% [w/v] peptone, 0.1% [w/v] tryptone, 0.1% [w/v] yeast extract, and 2.5% [w/v] glucose), *R. solanacearum* cells were collected by centrifugation at 16,000 × *g* for 5 min at room temperature and adjusted to the indicated absorbance at 600 nm (OD_{600}) with sterile water. Arabidopsis seeds were germinated on half-strength MS medium solidified with 0.8% agar (sigma). Seedlings were grown on vertically oriented half-strength MS plates for 7 days at 22 °C. For *R. solanacearum* inoculation, 7-day-old seedlings were transferred to new plates and moved to a growth chamber set to 27 °C for high-temperature acclimation for 1 day. This 1-day high-temperature treatment before *R. solanacearum* inoculation was used to minimize the effect of the higher temperature on Arabidopsis seedlings. Then, 10 μL of an *R. solanacearum* suspension at a titer of 1×10^7 colony-forming units (CFUs)/mL (OD_{600} = 0.01) was placed at a distance of 1 cm from the root tip. Phenotypes were observed daily. Each treatment contained at least 14 seedlings.

To evaluate the resistance phenotype of 4-week-old plants against *R. solanacearum* inoculation in soil, the plants were transferred from a 22 °C chamber to a 27 °C chamber for 1 day of acclimation. Before inoculation, a cut was made in the soil 1 cm away from the taproot, and 20 mL of *R. solanacearum* suspension (OD_{600} = 0.1) was poured onto the roots of the plants. The assay was performed in triplicate, using at least 10 Arabidopsis plants per treatment. The disease index was recorded daily according to a previously described scale from 0 to 4 (Deslandes et al. 1998). Briefly, disease severity was divided into the following levels: 0, all leaves are healthy; 1, 25% of the leaves have wilted; 2, about 50% of the leaves have wilted; 3, 75% of the leaves have wilted; 4, the whole plant is wilted. For inoculation of tomato and tobacco, individual 4-week-old plants were each inoculated with 10 mL of *R. solanacearum* suspension (OD_{600} = 0.1) onto the soil near the roots. The disease index was observed daily and scored as above.

RNA-seq analysis

RNA-Seq was performed by OE Biotech (Shanghai, China). Arabidopsis seedlings grown for 7 days were treated with GMI1000 at a concentration of OD_{600} = 0.01 for 18 h. Total RNA was isolated from Arabidopsis roots using the RNeasy Mini Kit (Qiagen), according to the manufacturer's instructions. RNA-seq library was prepared using the TruSeq RNA Sample Prep Kit v2 (Illumina, San Diego, CA, United States) and sequenced on the Illumina NovaSeq 6000 platform to generate 150 bp paired-end reads. Reads were quantified and mapped to the Arabidopsis reference genome (TAIR11) using the Salmon software (Patro et al. 2017). Differentially expressed genes (DEGs) were selected from the RNA-seq count data using the DESeq2 package (Love et al. 2014). All DEGs have been summarized (Supplementary Table S2). Enrichment analysis was performed using g:Profiler (Raudvere et al. 2019), and the data were visualized using R.

ChIP and qPCR

Roots of seedling grown on half-strength MS medium for 7 days were pooled for one replicate and three replicates were used. The ChIP assay was performed as previously described (Zhu et al. 2020). To determine gene expression, 0.3 μg purified DNA and input DNA (control) were subjected to qPCR using sequence-specific primers (Supplementary Table S1).

Electrophoretic mobility shift assay

Recombinant GST-RD26 protein and GST protein were used for the EMSA. When designing the fluorescent probe, FAM was added to the 5′ end of the F primer, the R primer was not modified, and the purification method was HPLC (TsingKe Biological Technology) (Supplementary Table S1). The DNA-RD2-binding reaction contained 100 pg probe, 200 ng GST-RD26 protein, 10 mM Tris-HCl [pH = 7.5], 5% [v/v] glycerol, 1 mM $MgCl_2$, 50 mM KCl, 0.2 mg/mL BSA, 0.5 mM DTT, 0.5 mg/mL polyglutamate, and the indicated amount of unlabeled competitor. The reactions were incubated

at 26 °C for 30 min and fractioned by electrophoresis in a 4% native polyacrylamide gel (acrylaminde:bisacrylamide, 29:1) containing 10% [v/v] glycerol, 89 mM Tris-HCl [pH = 8.0], 89 mM boric acid, and 2 mM EDTA. The FAM signal was detected using a fluorescence imager plate.

Dual-luciferase assay

The 2,000 bp promoter region upstream of lignin-related genes was cloned into pGreen-0800-LUC vector as the reporter plasmid (Supplementary Table S1). The effector plasmid 35S:*RD26* was constructed using pDT1 vector as described above. The reporter plasmid and effector plasmid were transformed into Arabidopsis protoplasts simultaneously. After 16 h of dark cultivation at 23 °C, samples were collected and subjected to dual-luciferase assay using the Dual-Luciferase Reporter Gene Assay Kit (RG027, Beyotime). The LUC and REN signals were detected using a Modulus Microplate Multimode Reader (Turner Biosystem). Three biological replicates were used for each sample, and similar results were obtained.

Phloroglucinol-HCl and basic fuchsin stainings

Phloroglucinol-HCl staining was performed at room temperature as previously described (Mitra and Loqué 2014). Seedlings were dehydrated in 100% ethanol overnight, rehydrated in a graded series of ethanol (75% [v/v], 50% [v/v], and 25% [v/v]) and water for 30 min each, followed by staining with 3% phloroglucinol (Sigma-Aldrich) dissolved in 30% [v/v] HCl for 1 min. The stained leaves and seedlings were observed under an optical microscope (Leica EZ4E). For simultaneous visualization of bacterial invasion and lignin deposition, a protocol adapted from Ursache et al. (2018) was used. Briefly, infected seedlings were fixated with 4% [v/v] paraformaldehyde (PFA) dissolved in 1× phosphate-buffered saline (PBS) solution for 1 h in vacuum, washed twice with 1× PBS and moved to a Clearsee solution overnight with gentle shaking at room temperature. Seedlings were stained with a solution of 0.2% [w/v] basic fuchsin dissolved in Clearsee and incubated 30 min with gentle shaking at room temperature, and thoroughly washed twice with Clearsee.

Histochemical staining of tomato and tobacco roots

Histochemical staining of silenced tomato and tobacco roots was performed by Wuhan servicebio technology (Wuhan, China). Briefly, roots of plants older than 4 weeks were separated from soil, washed with sterile water and fixed in Formalin-Aceto-Alcohol (FAA). Root tissues were stained for lignin using phloroglucinol-HCl after paraffin sectioning.

Lignin quantification assay

Lignin content was determined by the acetyl bromide-based method as previously described (Chang et al. 2008). About 70–80 mg of Arabidopsis root material grown for 7 days were accurately weighed and transferred to 80 °C for drying; about 3 mg of cell wall extract were weighed and used for lignin quantification with the Lignin Content Assay Kit (Beijing Boxbio Science & Technology Co. Ltd, Beijing, China). Lignin was quantified as described in the manufacturer's instructions. The prepared solutions were transferred to 96-well microplates, and the absorbance was measured using Microplate Reader at 280 nm. The extinction coefficient used for Arabidopsis was 23.35 mL/mg/cm.

Microscopy settings and image processing

Confocal laser scanning microscopy was performed on a Zeiss LSM880 inverted confocal scanning microscope. VENUS/GFP and PI were excited at 488 and 543 nm wavelength, respectively, with detection wavelengths of 578 to 718 nm and 493 to 555 nm. The detection digital gain is set to 1.0, and the laser intensity is 80–90%. For simultaneous visualization of bacterial invasion and lignin deposition, GFP was imaged using 488 nm excitation and detection at 500 to 550 nm and basic fuchsin 561 nm excitation and detection at 600 to 650 nm. Images were taken using a Leica SP5 confocal microscope. Photographs were taken with 20× objective. For more detailed analyses in large areas of interest, imaging was performed using Z-scan by FIJI (https://imagej.net/imagej-wiki-static/Fiji). Sequential scanning was used to avoid interference between fluorescence channels. Confocal images after treatments were taken following identical criteria. In each experiment, 10 homozygous seedlings are analyzed. The images in each group are processed with the same set of parameters.

Statistical analysis

The data are presented as mean ± SD. *n* represents individual biological replicates. Statistical significance was analyzed by two-tailed Student's *t*-test using Prism 9 software. $^{*}P < 0.05$, $^{**}P < 0.01$, $^{***}P < 0.001$; ns: not significant. The different lowercase letters indicate statistical significance (one-way ANOVA) by SPSS (version 27.0.0).

Accession numbers

Sequence data from this article can be found in the GenBank/EMBL/TAIR data libraries under accession numbers_ *FER* (At3g51550), *RD26* (At4g27410), *SlFER* (Solyc09g015830), *SlRD26* (also reported as *SlJA2*, Solyc12g013620), and *Ntfer* (Ntab0986670).

Acknowledgments

The authors would like to thank Dr. Jingshi Xue for providing *proPAL1:PAL1-VENUS* and *ccoaomt1* Arabidopsis seeds. We thank Dr. Xiaoyun Li for providing *rd26-2* seeds. We thank Fan Xu and other members from Feng Yu group for helpful discussions.

Author contributions

F.Y., D.W., and B.W. conceived the study; B.W., C.L. (Cailin Luo), X.L., J.C. (Jun Cai), J.C. (Jia Chen), Z.Z., Y.C., and A.J. performed the experiments; D.W., B.W., C.L. (Changsheng Li), C.Z., L.O., W.P., Y.P., and M.V. analyzed the data; F.Y., D.W., and B.W. wrote the article with input from all authors.

Supplementary data

The following materials are available in the online version of this article.

Supplementary Figure S1. Colonization of *R. solanacearum* in the xylem of Col-0 roots.

Supplementary Figure S2. The *fer-4* mutant is resistant to *R. solanacearum* inoculation.

Supplementary Figure S3. Disease phenotype of C24 and *srn*, an independent mutant of *FER* in the C24 background.

Supplementary Figure S4. Yeast two-hybrid assay confirming the specific interaction between FER and RD26.

Supplementary Figure S5. Spatial expression pattern of RD26-VENUS in *rd26 proMGT6:RD26-VENUS* roots.

Supplementary Figure S6. LC-MS/MS identification of RD26 phosphorylation sites following an in vitro phosphorylation assay.

Supplementary Figure S7. Stability and spatial expression pattern of RD26.

Supplementary Figure S8. Growth of *RD26*-OE, *rd26*, *rd26 fer-4*, and *fer-4 RD26*-OE lines.

Supplementary Figure S9. *fer-4* and *RD26*-OE share a similar transcriptional response in the absence of *R. solanacearum* infection.

Supplementary Figure S10. *fer-4* and *RD26*-OE share a similar transcriptional response upon *R. solanacearum* infection.

Supplementary Figure S11. RD26 is predicted to directly bind to the promoters of lignin-related genes.

Supplementary Figure S12. Lignin visualization and quantification in the xylem of Arabidopsis roots after *R. solanacearum* inoculation.

Supplementary Figure S13. Disease phenotype of the lignin biosynthesis mutant *ccoaomt1*.

Supplementary Figure S14. The FER–RD26 module regulates resistance to *R. solanacearum* in tomato and tobacco.

Supplementary Figure S15. Phenotype of resistance to *R. solanacearum* after silencing lignin-related genes in tomato.

Supplementary Table S1. Primers used in this study.

Supplementary Table S2. RNA-seq count data and differentially expressed genes lists.

Supplementary Data Set 1. Statistical data.

Funding

This work was financially supported by the Natural Science Foundation of China (32372485, 32070769, 32370757), the Natural Science Foundation of Hunan Province (2022JJ20008), the Science and Technology Program of Hunan Province (2021RC2061, 2022RC1166, 2023ZJ1080), the Young Elite Scientists Sponsorship Program by CAST (Grant No. 2021QNRC001), and the National Key Research and Development Program of China (2023YFD1401100). Research was also funded by grant MCIN/AEI/PID2019-108595RB-I00 and grant TED2021-131457B-I00 funded by MCIN/AEI and by the "European Union NextGenerationEU/PRTR" (to M.V.), through the "Severo Ochoa Programme for Centres of Excellence in R&D" (CEX2019-000917), and by the CERCA Program of the Catalan government (Generalitat de Catalunya).

Conflict of interest statement. The authors declare no competing interests.

Data availability

RNA-seq data generated in this study have been deposited to GEO with accession number PRJNA992763.

References

Chang M, Chen H, Liu F, Fu ZQ. PTI and ETI: convergent pathways with diverse elicitors. *Trends Plant Sci*. 2022:27(2):113–115. https://doi.org/10.1016/j.tplants.2021.11.013

Chang XF, Chandra R, Berleth T, Beatson RP. Rapid, microscale, acetyl bromide-based method for high-throughput determination of lignin content in *Arabidopsis thaliana*. *J Agric Food Chem*. 2008:56(16):6825–6834. https://doi.org/10.1021/jf800775f

Chen H, Zou Y, Shang Y, Lin H, Wang Y, Cai R, Tang X, Zhou JM. Firefly luciferase complementation imaging assay for protein-protein interactions in plants. *Plant Physiol*. 2008:146(2):368–376. https://doi.org/10.1104/pp.107.111740

Chen J, Yu F, Liu Y, Du C, Li X, Zhu S, Wang X, Lan W, Rodriguez PL, Liu X, et al. FERONIA interacts with ABI2-type phosphatases to facilitate signaling cross-talk between abscisic acid and RALF peptide in Arabidopsis. *Proc Natl Acad Sci USA*. 2016:113(37):E5519–E5527. https://doi.org/10.1073/pnas.1608449113

Chezem WR, Memon A, Li FS, Weng JK, Clay NK. SG2-type R2R3-MYB transcription factor MYB15 controls defense-induced lignification and basal immunity in arabidopsis. *Plant Cell*. 2017:29(8):1907–1926. https://doi.org/10.1105/tpc.16.00954

Chisholm ST, Coaker G, Day B, Staskawicz BJ. Host-microbe interactions: shaping the evolution of the plant immune response. *Cell*. 2006:124(4):803–814. https://doi.org/10.1016/j.cell.2006.02.008

Chuberre C, Plancot B, Driouich A, Moore JP, Bardor M, Gügi B, Vicré M. Plant immunity is compartmentalized and specialized in roots. *Front Plant Sci*. 2018:9:1692. https://doi.org/10.3389/fpls.2018.01692

Cui H, Tsuda K, Parker JE. Effector-triggered immunity: from pathogen perception to robust defense. *Annu Rev Plant Biol*. 2015:66(1):487–511. https://doi.org/10.1146/annurev-arplant-050213-040012

De La Fuente L, Merfa MV, Cobine PA, Coleman JJ. Pathogen adaptation to the xylem environment. *Annu Rev Phytopathol*. 2022:60(1):163–186. https://doi.org/10.1146/annurev-phyto-021021-041716

de Pedro-Jové R, Puigvert M, Sebastià P, Macho AP, Monteiro JS, Coll NS, Setúbal JC, Valls M. Dynamic expression of *Ralstonia solanacearum* virulence factors and metabolism-controlling genes during plant infection. *BMC Genomics*. 2021:22(1):170. https://doi.org/10.1186/s12864-021-07457-w

Deslandes L, Pileur F, Liaubet L, Camut S, Can C, Williams K, Holub E, Beynon J, Arlat M, Marco Y. Genetic characterization of RRS1, a recessive locus in *Arabidopsis thaliana* that confers resistance to the bacterial soilborne pathogen *Ralstonia solanacearum*. *Mol Plant Microbe Interact*. 1998:11(7):659–667. https://doi.org/10.1094/MPMI.1998.11.7.659

Do CT, Pollet B, Thévenin J, Sibout R, Denoue D, Barrière Y, Lapierre C, Jouanin L. Both caffeoyl coenzyme A 3-O-methyltransferase 1 and caffeic acid O-methyltransferase 1 are involved in redundant functions for lignin, flavonoids and sinapoyl malate biosynthesis in Arabidopsis. *Planta*. 2007:226(5):1117–1129. https://doi.org/10.1007/s00425-007-0558-3

Du C, Li X, Chen J, Chen W, Li B, Li C, Wang L, Li J, Zhao X, Lin J, et al. Receptor kinase complex transmits RALF peptide signal to inhibit root growth in Arabidopsis. *Proc Natl Acad Sci USA*. 2016:113(51):E8326–E8334. https://doi.org/10.1073/pnas.1609626113

Duan Q, Kita D, Li C, Cheung AY, Wu HM. FERONIA receptor-like kinase regulates RHO GTPase signaling of root hair development. *Proc Natl Acad Sci USA*. 2010:107(41):17821–17826. https://doi.org/10.1073/pnas.1005366107

Fan Y, Bai J, Wu S, Zhang M, Li J, Lin R, Hu C, Jing B, Wang J, Xia X, et al. The RALF2-FERONIA-MYB63 module orchestrates growth and defense in tomato roots. *New Phytol*. 2024:243(3):1123–1136. https://doi.org/10.1111/nph.19865

Feng W, Kita D, Peaucelle A, Cartwright HN, Doan V, Duan Q, Liu MC, Maman J, Steinhorst L, Schmitz-Thom I, et al. The FERONIA receptor kinase maintains cell-wall integrity during salt stress through Ca2+ signaling. *Curr Biol*. 2018:28(5):666–675.e5. https://doi.org/10.1016/j.cub.2018.01.023

Ferreira V, Pianzzola MJ, Vilaró FL, Galván GA, Tondo ML, Rodriguez MV, Orellano EG, Valls M, Siri MI. Interspecific potato breeding lines display differential colonization patterns and induced defense responses after *Ralstonia solanacearum* infection. *Front Plant Sci*. 2017:8:1424. https://doi.org/10.3389/fpls.2017.01424

Fucile G, Di Biase D, Nahal H, La G, Khodabandeh S, Chen Y, Easley K, Christendat D, Kelley L, Provart NJ. Eplant and the 3D data display initiative: integrative systems biology on the world wide web.

PLoS One. 2011:6(1):e15237. https://doi.org/10.1371/journal.pone.0015237

Fujita M, Fujita Y, Maruyama K, Seki M, Hiratsu K, Ohme-Takagi M, Tran LS, Yamaguchi-Shinozaki K, Shinozaki K. A dehydration-induced NAC protein, RD26, is involved in a novel ABA-dependent stress-signaling pathway. *Plant J*. 2004:39(6):863–876. https://doi.org/10.1111/j.1365-313X.2004.02171.x

Galindo-González L, Deyholos MK. RNA-seq transcriptome response of flax (*Linum usitatissimum* L.) to the pathogenic fungus *Fusarium oxysporum* f. sp. *lini*. *Front Plant Sci*. 2016:7:1766. https://doi.org/10.3389/fpls.2016.01766

Genin S, Denny TP. Pathogenomics of the *Ralstonia solanacearum* species complex. *Annu Rev Phytopathol*. 2012:50(1):67–89. https://doi.org/10.1146/annurev-phyto-081211-173000

Gluck-Thaler E, Cerutti A, Perez-Quintero AL, Butchacas J, Roman-Reyna V, Madhavan VN, Shantharaj D, Merfa MV, Pesce C, Jauneau A, et al. Repeated gain and loss of a single gene modulates the evolution of vascular plant pathogen lifestyles. *Sci Adv*. 2020:6(46):eabc4516. https://doi.org/10.1126/sciadv.abc4516

Guo H, Nolan TM, Song G, Liu S, Xie Z, Chen J, Schnable PS, Walley JW, Yin Y. FERONIA receptor kinase contributes to plant immunity by suppressing jasmonic acid signaling in *Arabidopsis thaliana*. *Curr Biol*. 2018:28(20):3316–3324.e6. https://doi.org/10.1016/j.cub.2018.07.078

Ishihara T, Mitsuhara I, Takahashi H, Nakaho K. Transcriptome analysis of quantitative resistance-specific response upon *Ralstonia solanacearum* infection in tomato. *PLoS One*. 2012:7(10):e46763. https://doi.org/10.1371/journal.pone.0046763

Jacobs JM, Babujee L, Meng F, Milling A, Allen C. The in planta transcriptome of *Ralstonia solanacearum*: conserved physiological and virulence strategies during bacterial wilt of tomato. *mBio*. 2012:3(4):e00114-12. https://doi.org/10.1128/mBio.00114-12

Jeon HS, Jang E, Kim J, Kim SH, Lee MH, Nam MH, Tobimatsu Y, Park OK. Pathogen-induced autophagy regulates monolignol transport and lignin formation in plant immunity. *Autophagy*. 2023:19(2):597–615. https://doi.org/10.1080/15548627.2022.2085496

Jones JD, Dangl JL. The plant immune system. *Nature*. 2006:444(7117):323–329. https://doi.org/10.1038/nature05286

Kashyap A, Planas-Marquès M, Capellades M, Valls M, Coll NS. Blocking intruders: inducible physico-chemical barriers against plant vascular wilt pathogens. *J Exp Bot*. 2021:72(2):184–198. https://doi.org/10.1093/jxb/eraa444

Kim SH, Lam PY, Lee MH, Jeon HS, Tobimatsu Y, Park OK. The Arabidopsis R2R3 MYB transcription factor MYB15 is a key regulator of lignin biosynthesis in effector-triggered immunity. *Front Plant Sci*. 2020:11:583153. https://doi.org/10.3389/fpls.2020.583153

Lee MH, Jeon HS, Kim SH, Chung JH, Roppolo D, Lee HJ, Cho HJ, Tobimatsu Y, Ralph J, Park OK. Lignin-based barrier restricts pathogens to the infection site and confers resistance in plants. *EMBO J*. 2019:38(23):e101948. https://doi.org/10.15252/embj.2019101948

Li C, He Q, Zhang F, Yu J, Li C, Zhao T, Zhang Y, Xie Q, Su B, Mei L, et al. Melatonin enhances cotton immunity to Verticillium wilt via manipulating lignin and gossypol biosynthesis. *Plant J*. 2019:100(4):784–800. https://doi.org/10.1111/tpj.14477

Lin H, Wang M, Chen Y, Nomura K, Hui S, Gui J, Zhang X, Wu Y, Liu J, Li Q, et al. An MKP-MAPK protein phosphorylation cascade controls vascular immunity in plants. *Sci Adv*. 2022:8(10):eabg8723. https://doi.org/10.1126/sciadv.abg8723

Liu C, Yu H, Rao X, Li L, Dixon RA. Abscisic acid regulates secondary cell-wall formation and lignin deposition in *Arabidopsis thaliana* through phosphorylation of NST1. *Proc Natl Acad Sci USA*. 2021:118(5):e2010911118. https://doi.org/10.1073/pnas.2010911118

Liu C, Yu H, Voxeur A, Rao X, Dixon RA. FERONIA and wall-associated kinases coordinate defense induced by lignin modification in plant cell walls. *Sci Adv*. 2023a:9(10):eadf7714. https://doi.org/10.1126/sciadv.adf7714

Liu HB, Li X, Cai J, Jiang LL, Zhang X, Wu D, Wang L, Yang A, Guo C, Chen J, et al. A screening of inhibitors targeting the receptor kinase FERONIA reveals small molecules that enhance plant root immunity. *Plant Biotechnol J*. 2023b:21(1):63–77. https://doi.org/10.1111/pbi.13925

Love MI, Huber W, Anders S. Moderated estimation of fold change and dispersion for RNA-seq data with DESeq2. *Genome Biol*. 2014:15(12):550. https://doi.org/10.1186/s13059-014-0550-8

Lowe-Power TM, Khokhani D, Allen C. How *Ralstonia solanacearum* exploits and thrives in the flowing plant xylem environment. *Trends Microbiol*. 2018:26(11):929–942. https://doi.org/10.1016/j.tim.2018.06.002

Lu H, Lema A S, Planas-Marquès M, Alonso-Díaz A, Valls M, Coll NS. Type III secretion-dependent and-independent phenotypes caused by *Ralstonia solanacearum* in Arabidopsis roots. *Mol Plant Microbe Interact*. 2018:31(1):175–184. https://doi.org/10.1094/MPMI-05-17-0109-FI

Mansfield J, Genin S, Magori S, Citovsky V, Sriariyanum M, Ronald P, Dow M, Verdier V, Beer SV, Machado MA, et al. Top 10 plant pathogenic bacteria in molecular plant pathology. *Mol Plant Pathol*. 2012:13(6):614–629. https://doi.org/10.1111/j.1364-3703.2012.00804.x

Meng SF, Zhang B, Tang RJ, Zheng XJ, Chen R, Liu CG, Jing YP, Ge HM, Zhang C, Chu YL, et al. Four plasma membrane-localized MGR transporters mediate xylem Mg2+ loading for root-to-shoot Mg2+ translocation in Arabidopsis. *Mol Plant*. 2022:15(5):805–819. https://doi.org/10.1016/j.molp.2022.01.011

Mitra PP, Loqué D. Histochemical staining of *Arabidopsis thaliana* secondary cell wall elements. *J Vis Exp*. 2014(87):e51381. https://doi.org/10.3791/51381

Monteiro F, Genin S, van Dijk I, Valls M. A luminescent reporter evidences active expression of *Ralstonia solanacearum* type III secretion system genes throughout plant infection. *Microbiology (Reading)*. 2012:158(Pt 8):2107–2116. https://doi.org/10.1099/mic.0.058610-0

Nakano Y, Yamaguchi M, Endo H, Rejab NA, Ohtani M. NAC-MYB-based transcriptional regulation of secondary cell wall biosynthesis in land plants. *Front Plant Sci*. 2015:6:288. https://doi.org/10.3389/fpls.2015.00288

Novo M, Silvar C, Merino F, Martínez-Cortés T, Lu F, Ralph J, Pomar F. Deciphering the role of the phenylpropanoid metabolism in the tolerance of *Capsicum annuum* L. to *Verticillium dahliae* Kleb. *Plant Sci*. 2017:258:12–20. https://doi.org/10.1016/j.plantsci.2017.01.014

Patro R, Duggal G, Love MI, Irizarry RA, Kingsford C. Salmon provides fast and bias-aware quantification of transcript expression. *Nat Methods*. 2017:14(4):417–419. https://doi.org/10.1038/nmeth.4197

Poueymiro M, Cunnac S, Barberis P, Deslandes L, Peeters N, Cazale-Noel AC, Boucher C, Genin S. Two type III secretion system effectors from *Ralstonia solanacearum* GMI1000 determine host-range specificity on tobacco. *Mol Plant Microbe Interact*. 2009:22(5):538–550. https://doi.org/10.1094/MPMI-22-5-0538

Poueymiro M, Genin S. Secreted proteins from *Ralstonia solanacearum*: a hundred tricks to kill a plant. *Curr Opin Microbiol*. 2009:12(1):44–52. https://doi.org/10.1016/j.mib.2008.11.008

Raudvere U, Kolberg L, Kuzmin I, Arak T, Adler P, Peterson H, Vilo J. g:Profiler: a web server for functional enrichment analysis and conversions of gene lists (2019 update). *Nucleic Acids Res*. 2019:47(W1):W191–W198. https://doi.org/10.1093/nar/gkz369

Rich-Griffin C, Eichmann R, Reitz MU, Hermann S, Woolley-Allen K, Brown PE, Wiwatdirekkul K, Esteban E, Pasha A, Kogel KH, et al.

Regulation of cell type-specific immunity networks in arabidopsis roots. *Plant Cell*. 2020:32(9):2742–2762. https://doi.org/10.1105/tpc.20.00154

Rotman N, Rozier F, Boavida L, Dumas C, Berger F, Faure JE. Female control of male gamete delivery during fertilization in *Arabidopsis thaliana*. *Curr Biol*. 2003:13(5):432–436. https://doi.org/10.1016/S0960-9822(03)00093-9

Sabella E, Luvisi A, Aprile A, Negro C, Vergine M, Nicolì F, Miceli A, De Bellis L. *Xylella fastidiosa* induces differential expression of lignification related-genes and lignin accumulation in tolerant olive trees cv. Leccino. *J Plant Physiol*. 2018:220:60–68. https://doi.org/10.1016/j.jplph.2017.10.007

Salanoubat M, Genin S, Artiguenave F, Gouzy J, Mangenot S, Arlat M, Billault A, Brottiert P, Camus JC, Cattolico L, et al. Genome sequence of the plant pathogen *Ralstonia solanacearum*. *Nature*. 2002:415(6871):497–502. https://doi.org/10.1038/415497a

Stegmann M, Monaghan J, Smakowska-Luzan E, Rovenich H, Lehner A, Holton N, Belkhadir Y, Zipfel C. The receptor kinase FER is a RALF-regulated scaffold controlling plant immune signaling. *Science*. 2017:355(6322):287–289. https://doi.org/10.1126/science.aal2541

Tran LS, Nakashima K, Sakuma Y, Simpson SD, Fujita Y, Maruyama K, Fujita M, Seki M, Shinozaki K, Yamaguchi-Shinozaki K. Isolation and functional analysis of Arabidopsis stress-inducible NAC transcription factors that bind to a drought-responsive cis-element in the early responsive to dehydration stress 1 promoter. *Plant Cell*. 2004:16(9):2481–2498. https://doi.org/10.1105/tpc.104.022699

Ursache R, Andersen TG, Marhavý P, Geldner N. A protocol for combining fluorescent proteins with histological stains for diverse cell wall components. *Plant J*. 2018:93(2):399–412. https://doi.org/10.1111/tpj.13784

Wang P, Clark NM, Nolan TM, Song G, Bartz PM, Liao CY, Montes-Serey C, Katz E, Polko JK, Kieber JJ, et al. Integrated omics reveal novel functions and underlying mechanisms of the receptor kinase FERONIA in *Arabidopsis thaliana*. *Plant Cell*. 2022:34(7):2594–2614. https://doi.org/10.1093/plcell/koac111

Wang Y, Zhao A, Morcillo RJL, Yu G, Xue H, Rufian JS, Sang Y, Macho AP. A bacterial effector protein uncovers a plant metabolic pathway involved in tolerance to bacterial wilt disease. *Mol Plant*. 2021:14(8):1281–1296. https://doi.org/10.1016/j.molp.2021.04.014

Xie M, Zhang J, Tschaplinski TJ, Tuskan GA, Chen JG, Muchero W. Regulation of lignin biosynthesis and its role in growth-defense tradeoffs. *Front Plant Sci*. 2018:9:1427. https://doi.org/10.3389/fpls.2018.01427

Xu F, Chen J, Li Y, Ouyang S, Yu M, Wang Y, Fang X, He K, Yu F. The soil emergence-related transcription factor PIF3 controls root penetration by interacting with the receptor kinase FER. *Dev Cell*. 2024:59(4):434–447.e8. https://doi.org/10.1016/j.devcel.2024.01.001

Xu H, Liu P, Wang C, Wu S, Dong C, Lin Q, Sun W, Huang B, Xu M, Tauqeer A, et al. Transcriptional networks regulating suberin and lignin in endodermis link development and ABA response. *Plant Physiol*. 2022:190(2):1165–1181. https://doi.org/10.1093/plphys/kiac298

Xue JS, Zhang B, Zhan H, Lv YL, Jia XL, Wang T, Yang NY, Lou YX, Zhang ZB, Hu WJ, et al. Phenylpropanoid derivatives are essential components of sporopollenin in vascular plants. *Mol Plant*. 2020:13(11):1644–1653. https://doi.org/10.1016/j.molp.2020.08.005

Yu F, Qian L, Nibau C, Duan Q, Kita D, Levasseur K, Li X, Lu C, Li H, Hou C, et al. FERONIA receptor kinase pathway suppresses abscisic acid signaling in Arabidopsis by activating ABI2 phosphatase. *Proc Natl Acad Sci USA*. 2012:109(36):14693–14698. https://doi.org/10.1073/pnas.1212547109

Yuan M, Ngou BPM, Ding P, Xin XF. PTI-ETI crosstalk: an integrative view of plant immunity. *Curr Opin Plant Biol*. 2021:62:102030. https://doi.org/10.1016/j.pbi.2021.102030

Zhang X, Peng H, Zhu S, Xing J, Li X, Zhu Z, Zheng J, Wang L, Wang B, Chen J, et al. Nematode-encoded RALF peptide mimics facilitate parasitism of plants through the FERONIA receptor kinase. *Mol Plant*. 2020a:13(10):1434–1454. https://doi.org/10.1016/j.molp.2020.08.014

Zhang X, Wang D, Chen J, Wu D, Feng X, Yu F. Nematode RALF-Like 1 targets soybean malectin-like receptor kinase to facilitate parasitism. *Front Plant Sci*. 2021:12:775508. https://doi.org/10.3389/fpls.2021.775508

Zhang X, Yang Z, Wu D, Yu F. RALF-FERONIA signaling: linking plant immune response with cell growth. *Plant Commun*. 2020b:1(4):100084. https://doi.org/10.1016/j.xplc.2020.100084

Zhang Y, Chen M, Siemiatkowska B, Toleco MR, Jing Y, Strotmann V, Zhang J, Stahl Y, Fernie AR. A highly efficient agrobacterium-mediated method for transient gene expression and functional studies in multiple plant species. *Plant Commun*. 2020c:1(5):100028. https://doi.org/10.1016/j.xplc.2020.100028

Zhong R, Demura T, Ye ZH. SND1, a NAC domain transcription factor, is a key regulator of secondary wall synthesis in fibers of Arabidopsis. *Plant Cell*. 2006:18(11):3158–3170. https://doi.org/10.1105/tpc.106.047399

Zhou F, Emonet A, Dénervaud Tendon V, Marhavy P, Wu D, Lahaye T, Geldner N. Co-incidence of damage and microbial patterns controls localized immune responses in roots. *Cell*. 2020:180(3):440–453.e18. https://doi.org/10.1016/j.cell.2020.01.013

Zhou J, Lee C, Zhong R, Ye ZH. MYB58 and MYB63 are transcriptional activators of the lignin biosynthetic pathway during secondary cell wall formation in Arabidopsis. *Plant Cell*. 2009:21(1):248–266. https://doi.org/10.1105/tpc.108.063321

Zhu S, Estévez JM, Liao H, Zhu Y, Yang T, Li C, Wang Y, Li L, Liu X, Pacheco JM, et al. The RALF1–FERONIA complex phosphorylates eIF4E1 to promote protein synthesis and polar root hair growth. *Mol Plant*. 2020:13(5):698–716. https://doi.org/10.1016/j.molp.2019.12.014

Zhu S, Fu Q, Xu F, Zheng H, Yu F. New paradigms in cell adaptation: decades of discoveries on the CrRLK1L receptor kinase signalling network. *New Phytol*. 2021:232(3):1168–1183. https://doi.org/10.1111/nph.17683